

SEX-DEPENDENT DIFFERENCES IN AMYLOID- $\beta$  ACCUMULATION IN A MOUSE  
MODEL OF ALZHEIMER'S DISEASE

by

Michael Gee

---

Copyright © Michael Gee 2021

A Thesis Submitted to the Faculty of the

GRADUATE INTERDISCIPLINARY PROGRAM IN PHYSIOLOGICAL SCIENCES

In Partial Fulfillment of the Requirements

For the Degree of

MASTER OF SCIENCE

In the Graduate College

THE UNIVERSITY OF ARIZONA

2021

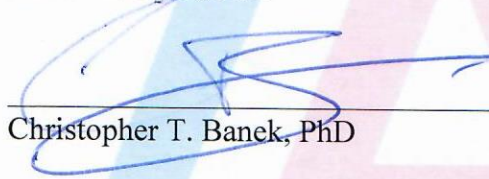
THE UNIVERSITY OF ARIZONA  
GRADUATE COLLEGE

As members of the Master's Committee, we certify that we have read the thesis prepared by Michael Gee, titled *Sex-Dependent Differences in Amyloid- $\beta$  Accumulation in a Mouse Model of Alzheimer's Disease* and recommend that it be accepted as fulfilling the dissertation requirement for the Master's Degree.



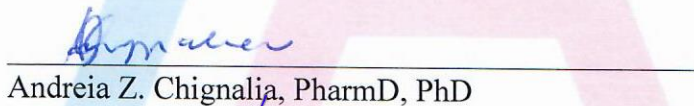
Paulo W. Pires, PhD

Date: 08/10/2021



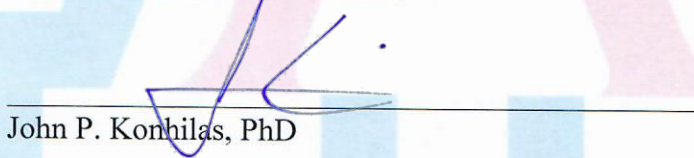
Christopher T. Banek, PhD

Date: 8/13/21



Andreia Z. Chignalia, PharmD, PhD

Date: 08/12/21



John P. Konhilas, PhD

Date: 16August2021

Final approval and acceptance of this thesis is contingent upon the candidate's submission of the final copies of the thesis to the Graduate College.

I hereby certify that I have read this thesis prepared under my direction and recommend that it be accepted as fulfilling the Master's requirement.



Paulo W. Pires, PhD  
Master's Thesis Committee Chair  
Physiological Sciences GIDP

Date: 8/16/21

## **Acknowledgements**

I would like to thank Dr. Paulo Pires for his mentorship and support throughout the project. Among many traits, Dr. Pires is enthusiastic and full of energy, yet also very patient. I also am grateful for the current and former lab members as well as those who I have worked with. Without them, I would not have been able to have the resources and knowledge to explore, develop, and troubleshoot different techniques. Not only that, but I also appreciate their companionship. Their interactions help to make each day new and exciting. I would also like to thank my committee members, Drs. Banek, Chignalia, and Konhilas for their patience, insight, and positivity. I am grateful that Dr. Banek allowed our lab to use his freezer to store samples. Additionally, I would like to thank the Dr. Fregosi as well as members of the Fregosi lab for allowing me to use their vibratome to produce brain slices. I would like to thank Dr. Gregory Rogers as well as Dan Buster for allowing me to use their microscope to take panoramas of stained tissues. I would also like to thank Kate Quinlan for answering any questions I had about the Physiological Sciences program in a very timely manner. I would also like to thank Professors Kelly Jackson and Jennifer Ravia as well as the Department of Nutritional Sciences for providing me the opportunity to assist with courses as well as financial assistance. I am also truly grateful to all my former mentors that have helped me get this far. Dr. Thomas Pannabecker introduced me to immunohistochemistry and helped foster that critical thinking that allowed me to be able to troubleshoot immunostaining experiments. Drs. Lukas, Whiteaker, and George as well as lab members such as their lab manager, Linda Lucero, introduced me to the molecular side of neuroscience and fostered my interest in neurodegenerative diseases. Last, but not least, I would also like to thank my family.

## Table of Contents

<b>List of Tables and Figures.....</b>	<b>5</b>
<b>Abstract.....</b>	<b>7</b>
<b>Introduction.....</b>	<b>8</b>
<b>Materials and Methods.....</b>	<b>15</b>
<b>Animals.....</b>	<b>15</b>
<b>Perfusion-Fixation.....</b>	<b>16</b>
<b>Thioflavin-T Histochemical Staining.....</b>	<b>17</b>
<b>Immunohistochemistry (IHC).....</b>	<b>17</b>
<b>Image Analysis.....</b>	<b>19</b>
<b>Statistical Analysis.....</b>	<b>21</b>
<b>Results.....</b>	<b>22</b>
<b>Discussion.....</b>	<b>43</b>
<b>References.....</b>	<b>51</b>

## List of Tables and Figures

<b>Table 1.</b> <i>Primers used to genotype 5x-FAD mice.....</i>	<b>15</b>
<b>Figure 1.</b> <i>Representative image of gel to discern wild-type from 5x-FAD mice.....</i>	<b>16</b>
<b>Figure 2.</b> <i>Thioflavin-T Staining of mouse brain slices.....</i>	<b>23</b>
<b>Figure 3.</b> <i>Thioflavin-T plaque density in cortex of 3-month-old 5x-FAD mice.....</i>	<b>24</b>
<b>Figure 4.</b> <i>Thioflavin-T plaque density in hippocampus of 3-month-old 5x-FAD mice.....</i>	<b>24</b>
<b>Figure 5.</b> <i>A<math>\beta</math>-pE3 is localized to the core of A<math>\beta</math> plaques.....</i>	<b>26</b>
<b>Figure 6.</b> <i>A<math>\beta</math>-pE3 plaque density in cortex of 3-month-old 5x-FAD mice.....</i>	<b>26</b>
<b>Figure 7.</b> <i>A<math>\beta</math>-pE3 plaque density in the hippocampus of 3-month-old 5x-FAD mice.....</i>	<b>27</b>
<b>Figure 8.</b> <i>Density and percent of A<math>\beta</math> plaques positive for A<math>\beta</math>-pE3 in the cortex of 3-month-old 5x-FAD mice.....</i>	<b>28</b>
<b>Figure 9.</b> <i>Density and percent of A<math>\beta</math> plaques positive for A<math>\beta</math>-pE3 in the hippocampus of 3-month-old 5x-FAD mice.....</i>	<b>29</b>
<b>Figure 10.</b> <i>1- and 2-month-old 5x-FAD male and female mice have few thioflavin-T reactive A<math>\beta</math> plaque accumulation in the cortex.....</i>	<b>32</b>
<b>Figure 11.</b> <i>1- and 2-month-old 5x-FAD male and female mice have few thioflavin-T reactive A<math>\beta</math> plaque accumulation in the hippocampus.....</i>	<b>33</b>
<b>Figure 12.</b> <i>A<math>\beta</math> antibody detects plaques in 2-, but not 1-month old, 5x-FAD male and female in the cortex.....</i>	<b>34</b>
<b>Figure 13.</b> <i>A<math>\beta</math> antibody detects few plaques in 2-, but not 1-month-old, 5x-FAD male and female mice in the hippocampus.....</i>	<b>35</b>

**Figure 14.** *Aβ-pE3 plaques are present in 2-, but not 1-month old, 5x-FAD male and female in the cortex.....36*

**Figure 15.** *Few Aβ-pE3 plaques are present in 2-, but not 1-month-old, 5x-FAD male and female in the hippocampus.....37*

**Figure 16.** *Relative collagen IV volume is unchanged between 3-month-old wild-Type and 5x-FAD male and female mice.....38*

**Figure 17.** *Number of capillaries is unchanged between 3-month-old Wild-Type and 5x-FAD male and female mice.....39*

**Figure 18.** *No accumulation of Aβ-pE3 is observed on parenchymal microvasculature of 3-month-old wild-type mice.....41*

**Figure 19.** *Low accumulation of Aβ-pE3 on the parenchymal microvasculature of 3-month-old 5x-FAD mice without sex differences.....41*

**Figure 20.** *No perivascular Aβ accumulation in the pial circulation of 3-month-old wild-type mice.....42*

**Figure 21.** *Perivascular Aβ accumulation in the pial circulation is not dependent on biological sex.....43*

## **Abstract**

Alzheimer's disease (AD) is a common cause of dementia and has a higher incidence in females. One of the pathological hallmarks of AD is the abnormal accumulation of amyloid- $\beta$  ( $A\beta$ ) plaques in the brain, which ultimately results in cognitive decline. It has been hypothesized that the accumulation of  $A\beta$  is facilitated by a modified form of  $A\beta$ , referred to as pyroglutamate  $A\beta$  ( $A\beta$ -pE3), which forms the core of  $A\beta$  plaques. Additionally, most AD patients display cerebral amyloid angiopathy (CAA), where  $A\beta$  accumulates around vessels of the brain. CAA can lead to a reduction in capillary number referred to as capillary rarefaction. This could reduce blood flow to the brain and contribute to the AD-associated cognitive decline. Whether the underlying mechanisms behind the higher incidence of AD in females involve sex differences in  $A\beta$ ,  $A\beta$ -pE3, CAA, or capillary rarefaction is not clear. Thus, we used histological techniques to characterize the *5x-FAD* mouse model of  $A\beta$  accumulation independently of aging to determine if differences in  $A\beta$  or  $A\beta$ -pE3 accumulation, CAA, and capillary rarefaction vary by sex in AD. At 3 months of age, there was no sex difference in  $A\beta$  plaque density and coverage in the cortex and hippocampus of *5x-FAD* mice. However, female *5x-FAD* mice displayed a significantly higher  $A\beta$ -pE3 plaque density, coverage, and percentage of  $A\beta$ -pE3-cored plaques in those same regions. No sex differences in  $A\beta$  and  $A\beta$ -pE3 plaque density was observed in 1- and 2-month-old *5x-FAD* mice. No differences were observed in blood vessel volume or capillary number when comparing 3-month-old *5x-FAD* male and female mice to their wild-type littermates. Additionally, CAA was present on the pial vessels and, to a lesser extent, parenchymal vessels of 3-month-old *5x-FAD* mice without sex differences. Thus, 3-month-old *5x-FAD* mice display sex differences in  $A\beta$ -pE3, but not overall  $A\beta$  accumulation, CAA, or capillary rarefaction. This sex difference in  $A\beta$ -pE3 seemed to not be present in 1- and 2-month-old *5x-FAD* mice. Although 3-month-old female *5x-FAD* mice had an elevated  $A\beta$ -pE3 load, no capillary rarefaction and parenchymal CAA was observed. This suggests that the microvasculature of these mice is unaffected, at least at the age studied. Future studies are aimed at assessing possible sex differences in the function of these vessels.

## **Introduction**

Alzheimer's disease (AD) is one of the primary types of dementia, and in 2020, 5.8 million Americans aged 65 and older are estimated to be living with AD, a number predicted to increase to 13.8 million by 2050<sup>1</sup>. This also poses an economic burden as the cost of AD and related dementias in the United States was estimated to be \$305 billion in 2020 and expected to rise with the increased aging population<sup>2</sup>. It is becoming clear that AD has higher incidence in age-matched women compared to men, particularly beyond 80 years of age<sup>3-8</sup>. According to the Alzheimer's Association, in the United States almost 2/3 of AD cases are in women<sup>2</sup>. However, it should be noted that this sex difference observation remains controversial, as some studies report the lack of difference<sup>9,10</sup> or even higher AD incidence in age-matched men compared to women<sup>11</sup>.

AD is characterized clinically by cognitive decline and neuro-pathologically by the presence of extracellular amyloid- $\beta$  (A $\beta$ ) plaques and neurofibrillary tangles, which are aggregate of hyperphosphorylated tau protein within neurons<sup>12</sup>. Although the clinical manifestations of AD may vary, common behaviors associated with the cognitive decline include memory loss, difficulty with planning and/or problem solving, trouble completing familiar tasks, impaired recognition of space or time, impaired visuospatial comprehension, difficulty with conversation, frequent inability to retrace steps, impaired judgement, less engagement in work or social activities, and changes in mood or personality<sup>13</sup>. Atrophy of brain regions such as the hippocampus, neocortex, entorhinal cortex, and several subcortical structures such as the basal ganglia have been observed in AD patients<sup>14</sup>. When taking sex into account, several studies observed that decline in certain aspects of cognition such as verbal memory is more pronounced in AD women compared to AD men<sup>15,16,20</sup>. Also, some studies suggest that brain atrophy is more severe in AD women compared to AD men<sup>17-19,20</sup>.

Although the cause of AD is not fully clear, one of the prevailing hypotheses, called the "amyloid cascade" hypothesis, posits that the aggregation of A $\beta$  is the causative agent that leads to cell death, neurofibrillary tangles, vascular damage, and dementia<sup>21</sup>. A $\beta$  is a peptide derived from enzymatic

processing of the membrane-bound amyloid precursor protein (APP) by  $\beta$ - and  $\gamma$ -secretases<sup>22</sup>. APP is primarily expressed in central neurons, with a lower expression in select neuronal and non-neuronal tissue in the periphery<sup>23</sup>. Some studies also suggest that APP can be expressed in glial cells<sup>23-25</sup> and brain endothelial cells<sup>24,25</sup>. The imprecise cleavage of APP by  $\gamma$ -secretase has been suggested to play a major role in generation of different A $\beta$  variants by mechanisms not yet fully elucidated<sup>26</sup>. However, mutations in proteins that comprise the  $\gamma$ -secretase complex, such as presenilin 1 (PSEN1) and 2 (PSEN2), in conjunction with mutations in APP, can elevate the production of pathologic forms of A $\beta$ <sup>27,26,22</sup>. Most mutations in APP occur near secretase-cleaving sites and near the A $\beta$  peptide sequence<sup>28</sup>. Such mutations include the Swedish mutation, which is located near the  $\beta$ -secretase cleavage site and is one of the APP mutations that results in increased A $\beta$  production<sup>28</sup>. Other mutations such as the London and Florida mutations, are located near the  $\gamma$ -secretase cleavage site and likewise result in increased A $\beta$  production<sup>28</sup>. The two most abundant variants associated with AD are A $\beta$ <sub>1-40</sub> and A $\beta$ <sub>1-42</sub>, which comprise of 40 and 42 amino acids respectively<sup>22</sup>. A $\beta$ <sub>1-40</sub> is a more soluble form and primarily found as perivascular deposits, also referred to as cerebral amyloid angiopathy (CAA)<sup>26</sup>. On the other hand, A $\beta$ <sub>1-42</sub> is less soluble<sup>29</sup> and is the main component of parenchymal plaques, also referred to as senile plaques<sup>22</sup>. It is important to note that A $\beta$ <sub>1-42</sub> can also be found in vascular deposits in leptomeningeal and parenchymal arterioles of AD patients, along with A $\beta$ <sub>1-40</sub><sup>30</sup>. The Swedish mutation has been observed to result in production of both A $\beta$ <sub>1-40</sub> and A $\beta$ <sub>1-42</sub><sup>31</sup>. However, the London and Florida mutations have been observed to result in a greater production of the A $\beta$ <sub>1-42</sub> variant with little to no effect on the production of A $\beta$ <sub>1-40</sub><sup>32</sup>. Despite the importance of A $\beta$  in the pathophysiology of AD, it remains controversial if A $\beta$  levels show sex differences. Some studies report no sex differences<sup>35,33</sup> or potentially greater plaque burden in females<sup>35</sup>. One human study also notes a greater degree of CAA in males compared to females<sup>36</sup>. Nonetheless, sex differences in A $\beta$  among the AD population has not been thoroughly explored and any discrepancies in the few studies that do attempt to explore those differences could be attributed to a number of factors such as differences in study designs and techniques used to acquire data<sup>20</sup>.

Early studies have attempted to identify and isolate the major species of A $\beta$  that comprised the core of senile plaques from postmortem brain samples of AD and Down Syndrome patients<sup>37</sup>. Such studies noted that the species that comprised the core of these plaques had a peptide sequence almost identical to A $\beta$  but possessed a truncated N-terminus and began with a phenylalanine at position 4<sup>37</sup>. Subsequent studies attempted to sequence the N-terminus of this peptide, with limited success. This observation, however, led to the hypothesis that the N-terminus of this species is blocked and cannot be accessed without proteolytic digestion<sup>38,39</sup>. A later study by Mori *et al.* successfully elucidated the sequence of this species using proteolytic treatment with pyroglutamylpeptidase and observed that it possessed a pyroglutamate at position 3<sup>40</sup>. This pyroglutamate has made this species resistant to degradation, preventing it from being sequenced in prior studies<sup>37-39</sup>. However, once its sequence was elucidated, further characterization of this isoform was possible<sup>39</sup>. This isoform, now referred to as pyroglutamate A $\beta$  (A $\beta$ -pE3), is derived from A $\beta$  species that have been modified by an enzyme called glutaminyl cyclase (QC)<sup>41</sup>. This enzyme is also involved in post-translational modification of several hormones via cyclizing amino-terminal glutaminyl residues into pyroglutaminyl residues<sup>42</sup>. Additionally, QC has been suggested to be elevated in the cortex of AD patients compared to non-AD patients<sup>43</sup>. The conversion of A $\beta$  to A $\beta$ -pE3 is initiated by removal of two charged amino acids from the N-terminus of the A $\beta$  peptide<sup>39</sup>. Some potential enzymes that have been suggested to accomplish this are aminopeptidase A<sup>44</sup>, mephrin  $\beta$ <sup>45</sup>, and dipeptidyl peptidase IV<sup>46</sup>, however, the identity of the enzyme(s) involved is unknown<sup>39</sup>. After removal of the two amino acids at the N-terminus, QC catalyzes the formation of a pyroglutamyl lactam ring at the amino terminal which makes A $\beta$ -pE3 more hydrophobic and resistant to degradation compared to the full length A $\beta$ <sup>39,47</sup>. A number of *in vitro* studies show that A $\beta$ -pE3 forms highly stable beta sheets<sup>48</sup>, possesses a higher aggregation propensity<sup>48</sup>, display rapid fibril formation<sup>49</sup>, and are more resistant to degradation<sup>50</sup> compared to A $\beta$ <sub>1-40</sub> and A $\beta$ <sub>1-42</sub>, suggesting this may be a potential seeding species for A $\beta$  plaques<sup>49</sup>. Additionally, the observations that this species forms the core of plaques<sup>47</sup> and that A $\beta$ -pE3 is the primary constituent of diffuse plaques, one of the earliest phases of amyloid deposition<sup>51</sup>, further support the hypothesis that A $\beta$ -pE3 may play a major role in initiating and/or facilitating the accumulation of neurotoxic A $\beta$  plaques in AD. Although A $\beta$ -pE3 levels

have been shown to be elevated in AD brains compared to non-cognitively impaired controls<sup>43,52,53</sup>, limited studies compared AD males versus AD females, and those that performed such analysis reported an absence of sex differences<sup>53,54</sup>. Interestingly, one human study notes that plasma QC activity may be higher in AD females, but not AD males<sup>55</sup>. Another study looking at QC levels in peripheral mononuclear cells noted elevated QC mRNA in the AD group compared to the control group, without sex differences<sup>56</sup>. However, given the small sample sizes of the above studies<sup>43,53-56</sup>, it is difficult to conclude whether sex differences exist in A $\beta$ -pE3 levels or QC processing of A $\beta$ . Thus, whether there are sex differences in accumulation of A $\beta$ -pE3 has not been satisfactorily explored.

Another factor that may contribute to further accumulation of A $\beta$  plaques in the brain parenchyma of in AD and subsequent neuronal cell death is neurovascular dysfunction as a consequence of a reduction in capillary density, referred to as capillary rarefaction<sup>57,58</sup>. A $\beta$  aggregates around the blood vessels of the brain, particularly the capillaries as CAA, resulting in narrowing or damage to the blood vessel which can contribute to reduced blood flow to the brain<sup>59,60</sup>. Histological analyses have observed that AD patient brains have altered capillary morphology<sup>61,62</sup> as well as reduced capillary density<sup>62-64</sup>. However, there are some studies that did not observed any significant changes in capillary density between AD patients and elderly controls<sup>61,65,66</sup> and some even reported greater capillary densities<sup>67-69</sup>. The variability in these observations<sup>61-63,65-69</sup> could be due to several factors such as relatively small sample sizes and differences in experimental procedures. Additionally, microbleeds, which are hemorrhagic lesions on cerebral microvessels associated with CAA<sup>70,71</sup>, were suggested to be present in 18- 32% of those with AD<sup>72</sup>. Further, capillary CAA comprises up to 30% of CAA cases<sup>74,75</sup> and seems to better correlate with AD pathology compared to general CAA, which includes A $\beta$  deposits on larger vessels such as arteries<sup>76</sup>. Additionally, capillary CAA has been associated with hippocampal microinfarcts and decline in cognitive functions<sup>77</sup>. Histological analysis of CAA in different cerebral blood vessels suggest that the capillaries play an important role in elimination of A $\beta$  via a perivascular route whereby A $\beta$  enters the perivascular drainage primarily at the level of the capillaries<sup>78</sup>, which could leave capillaries particularly susceptible to A $\beta$  accumulation.

Associations have been observed between capillary CAA, capillary damage, and cognitive decline; however, the role of CAA and microvascular rarefaction in AD needs further exploration.

The cerebral circulation is organized in such a way that the high metabolic demands of the brain are met<sup>79</sup>, and small perfusion deficits along any segment of the cerebral circulation, such as capillary rarefaction and/or CAA, are associated with neurodegenerative diseases such as AD<sup>80</sup>. Despite its relative small size (approximately 2% of total body weight in a healthy adult), the brain receives approximately 15-20% of the cardiac output<sup>79</sup>. Once blood leaves the left ventricle of the heart during systole, it travels through the aorta, which branches into the brachiocephalic, the left common carotid, and the left subclavian arteries<sup>81</sup>. The brachiocephalic artery then gives rise to the right common carotid and right subclavian arteries<sup>81</sup>. The subclavian arteries then give rise to the vertebral arteries<sup>81</sup>. The left and right carotid arteries then divide into the external (perfusion to the neck and face) and internal carotid arteries<sup>81</sup>. The vertebral arteries conduct blood to the base and posterior regions of the brain, accounting for approximately 20% of total blood flow<sup>81</sup>. On the other hand, internal carotid arteries conduct blood to more anterior regions, accounting for approximately 80% of total brain perfusion<sup>81</sup>. Near the base of the brain, the vertebral arteries converge to form the basilar artery, which then form an anastomotic ring with the internal carotid arteries named the Circle of Willis<sup>79,81</sup>. The Circle of Willis then gives rise to the anterior, middle, and posterior cerebral arteries which give rise to smaller arteries and arterioles that run along the surface of the brain, called the *pial* or *leptomeningeal circulation*<sup>79,81</sup>. The segments of the anterior cerebral artery primarily supply the frontal lobed and parts of the parietal lobes<sup>81</sup>. The medial cerebral artery supplies most of the lateral and ventral regions of the brain as well as deeper regions<sup>81</sup>, such as portions of the temporal and parietal lobes and basal ganglia<sup>81</sup>. The posterior cerebral artery primarily supplies blood to inferior and medial regions of the brain such as the occipital lobe and portions of the temporal and parietal lobes<sup>81</sup>. The pial vessels form a network of collaterals such that occlusion of one pial vessel does not drastically decrease cerebral blood flow and is virtually asymptomatic<sup>79</sup>. Branching from the pial arteries and diving into the brain at an almost 90° angle are the *penetrating arterioles*<sup>79</sup>. These arterioles are considered “bottlenecks”

of the cerebral microcirculation, as they do not exhibit extensive branching and occlusion of a single penetrating arteriole result in a drastic reduction in blood flow to that particular vascular territory and a detectable ischemic lesion<sup>82</sup>. These penetrating arterioles then give rise to parenchymal arterioles as they dive deeper into the brain and become almost completely ensheathed by astrocytic end-feet<sup>79</sup>. Capillaries branch out of parenchymal arterioles, which are also ensheathed by the astrocytic end-feet<sup>79</sup>. In a normal, healthy brain, it has been estimated that each neuron has its own capillary<sup>83,79</sup> that is always perfused with blood<sup>84,79</sup>. Unlike the arteries and arterioles, cerebral capillaries do not possess smooth muscle cells, but cells hypothesized to possess contractile-like properties called pericytes have been observed on these capillaries<sup>85,79</sup>. Blood leaving the capillaries then enters the post-capillary venules and drains into superficial veins located on the pial surface and deep or central veins located within the brain parenchyma<sup>79</sup>. All of these vessels are encased in a basal lamina comprised of extracellular matrix proteins such as collagen IV, heparin sulfate proteoglycans, laminin, and fibronectin<sup>84,79</sup>.

One unique aspect of the cerebral circulation is that a greater proportion of the vascular resistance lies in larger pial arteries<sup>79</sup>. Pressure gradient measurements of different sections of the cerebral circulation suggests that approximately 50% of the vascular resistance may be attributed to the internal carotid, vertebral, and pial arteries<sup>86,79</sup>, in contrast to the vasculature of most organs, where the major site of vascular resistance lies in the arterioles which smaller than 100  $\mu\text{m}$  in diameter<sup>87,79</sup>. Thus, in the brain, both larger arteries and small arterioles greatly influence vascular resistance and tissue perfusion distribution<sup>79</sup>. In the AD brain, CAA present on resistance arteries / arterioles contributes to degeneration of the smooth muscle layer, which can potentially lead to ruptures in the blood vessel wall and impaired regulation of local perfusion<sup>88,83</sup>. Additionally, A $\beta$  itself has been observed to induce vasoconstriction<sup>89,83</sup>, although it is unlikely that such occurs in extracranial arteries, as they do not display CAA<sup>83</sup>. Thus, the presence of CAA on pial arteries, penetrating and parenchymal arterioles, may contribute to impaired regulation of cerebral blood flow and, in the long-term, cognitive decline.

Mouse models have proven valuable as a pre-clinical model to study AD. Although the majority of AD cases are sporadic late onset, many of these mouse models rely on genetic mutations associated with familial AD (FAD), with the rationale being that events downstream of the initial trigger are similar<sup>90,91</sup>. Additionally, rodents do not naturally develop A $\beta$  plaques, thus, to recapitulate the disease pathology, transgenic manipulation is needed<sup>92</sup>. Oftentimes, these mice possess mutations in the APP gene, such as the PDAPP, Tg2576, APP23, J20, and TgCrND8, and, in some models, also PSEN1 and PSEN2, such as the *APP/PS1*, *5x-FAD*, and *3x-TgAD* mice, all of which result in overproduction of A $\beta$ <sup>93,91,92</sup>. The characteristics that differentiate these mouse models pertain to the gene constructs used such as the type of promoter used and the mutations in the APP genes<sup>91,93</sup>. Despite the ability to induce A $\beta$  plaque deposition in these mice models, there are several caveats that are important to consider. These mouse models may not fully recapitulate the entire AD process, thus caution is warranted when choosing which model to use<sup>91-93,90</sup>. Most of these mouse models harbor mutations associated with familial or early onset AD, which has been reported to comprise roughly 5% of total AD cases<sup>94</sup>, whereas the remaining 95% of AD cases are sporadic or late onset<sup>90-92,94</sup>. Also, another major drawback to these animal models is that there is no one model that harbors all aspects of AD<sup>93</sup>. For example, many mouse models only recapitulate A $\beta$  accumulation and do not accumulate hyperphosphorylated tau, although a model of both exists, which is the *3x-TgAD* model<sup>92,93</sup>. Additionally, overexpression of APP in these murine models may result in artificial protein interactions or physiological artifacts not normally observed in AD<sup>91-93</sup>. Nonetheless, these mouse models prove to be useful for identification of novel drugs for or cellular pathways involved in AD<sup>93,92</sup>. Several AD mouse models display sex differences whereby females are more prone to plaque accumulation and displaying earlier onset of pathology than their male counterparts<sup>95</sup>. However, not all AD mouse models display this sex difference, and, in some models, males have been reported to have a greater baseline plaque load compared to females<sup>96</sup>.

Thus, the objective of this study was to assess whether the higher incidence of AD in females correspond with greater accumulation of A $\beta$ , A $\beta$ -pE3, CAA, and capillary rarefaction. We hypothesize that

the greater incidence of AD in females may reflect an exacerbated accumulation of A $\beta$  and A $\beta$ -pE3, CAA, and capillary rarefaction compared to males. To determine whether sex differences may influence A $\beta$ , A $\beta$ -pE3, CAA, and capillary rarefaction, these sets of experiments will seek to characterize these different aspects of AD in a mouse model of AD. These findings may provide insight into the mechanisms and processes may account for the sex differences in AD. Furthermore, these experiments can provide information that can help further characterize the mouse model used.

## **Materials and Methods**

### ***Animals***

*5x-FAD* mice (Jackson Labs, strain 34840-JAX) are a model of early-onset familial Alzheimer's disease (FAD). These mice harbor five FAD-related mutations: the Swedish (K670N/M671L), Florida (I716V), and London (V717I) mutations associated with human APP as well as M146L and L286V mutations associated with PSEN1 under the transcriptional control of the neuron specific Thy1 promoter<sup>97</sup>. These mutations contribute to the rapid amyloid- $\beta$  accumulation, which makes these *5x-FAD* mice a useful model for amyloid deposition observed in AD. Mice used were bred on a C57bl/6J background and non-transgenic littermates were used as controls. Mice were genotyped by PCR analysis of tail clippings using primers listed in Table 1 (Figure 1).

Name	Primer Sequence (5' to 3')
<i>5x-FAD</i> Common	ACC CCC ATG TCA GAG TTC CT
<i>5x-FAD</i> WT Reverse	TAT ACA ACC TTG GGG GAT GG
<i>5x-FAD</i> Mutant Reverse	CGG GCC TCT TCG CTA TTA C

**Table 1.** Primers used to genotype *5x-FAD* mice.

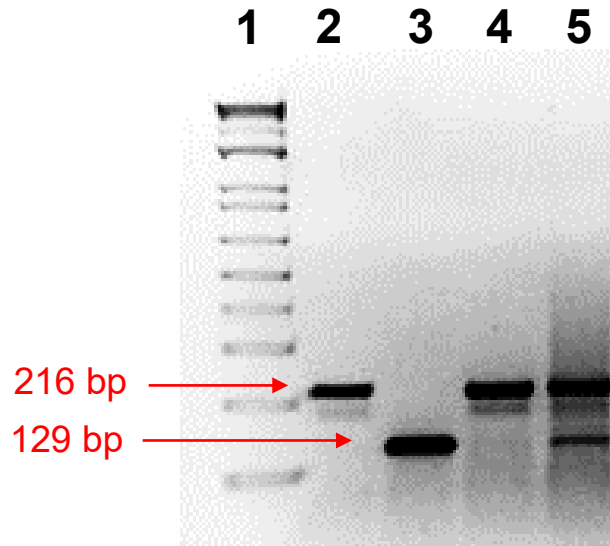


**Figure 1.** Representative image of gel to discern wild-type from *5x-FAD* mice. Lane 1 contains a DNA ladder used to determine base pair (bp) size of the DNA bands. Samples containing a band exclusively at 216 bp are wild-type (Lanes 2 and 4). Samples containing a band exclusively at 129 bp are homozygous mutant *5x-FAD* (Lane 3). Samples containing a band at 216 and 129 bp are hemizygous *5x-FAD* (Lane 5).

### ***Perfusion-fixation***

*5x-FAD* and wild-type mice were euthanized with pentobarbital (80mg/kg, intraperitoneal, Vortech Pharmaceuticals, Dearborn, MI) at 3 months of age. Mice were transcardially perfused with phosphate buffered saline (PBS) containing *cis*-diltiazem hydrochloride (10  $\mu$ mol/L, Millipore Sigma, D2521) and 1 unit/mL heparin, followed by perfusion with 4% paraformaldehyde. Brains were excised, post-fixed in 4% paraformaldehyde at room temperature overnight, and then washed with PBS before storage at 4°C. Brains were then sectioned on a Leica VT1000P vibratome to obtain 50  $\mu$ m-thick coronal sections. Sections were collected in PBS and stored at 4°C.

### ***Thioflavin-T Histochemical Staining***

For thioflavin-T staining, 50  $\mu\text{m}$  coronal sections were permeabilized in 0.1% Triton X-100 for 2 hours, treated with 15% formic acid for 15 minutes, and then washed with PBS. The sections were then treated with 0.5% sodium borohydride followed by 3 washes with PBS. The sections were then incubated in 5% horse serum, 0.1% Triton X-100 in PBS. After these treatments, the sections are incubated in a 0.5% thioflavin-T solution for 10 minutes, protected from light and then subsequently washed with 80% ethanol, 95% ethanol, and then PBS prior to mounting onto a slide<sup>98</sup>.

### ***Immunohistochemistry (IHC)***

Free-floating sections from wild-type and *5x-FAD* mice were processed for immunohistochemistry in parallel at room temperature. Sections underwent antigen retrieval using 10 mM Tris-sodium citrate pH 8.5 at 80°C for 1.5 hours, and then cooled to room temperature for 10 minutes before being washed with PBS. The sections were permeabilized in 0.1% Triton X-100 in PBS for 2 hours on a shaker at room temperature. Then, they underwent treatment with 15% formic acid in PBS for 15 minutes to enhance A $\beta$  staining and subsequently washed with PBS. Slices then underwent 0.5% sodium borohydride treatment for 15 minutes to reduce background fluorescence and then washed with PBS. After the sodium borohydride treatment and associated washes, slices were incubated in blocking solution comprised of 5% horse serum, 0.1% Triton X-100 in PBS for 1 hour prior to incubation with a rabbit polyclonal antibody against pyroglutamate amyloid- $\beta$  (1:1000, Synaptic Systems, Göttingen, Germany, catalog# 218 003) and a goat polyclonal antibody against collagen IV (1:1000, Novus Biologicals, Centennial, CO, catalog# NBP1-26549) for approximately 48 hours at 4°C. Sections were then washed with PBS prior to secondary antibody incubation with donkey anti-goat Alexa Fluor 594 (1:500, Jackson ImmunoResearch, catalog# 705-585-147) and donkey anti-rabbit Alexa Fluor 488 (1:500, Jackson ImmunoResearch, catalog# 711-545-152) diluted in a solution of 2% horse serum, 0.1% Triton X-100 in PBS for 2 hours. Brain sections were then

washed with PBS, and then mounted onto glass slides using the Fluoroshield with p-phenylenediamine (PPD) to preserve the fluorescence signal.

For immunolabeling of A $\beta$  in the pial vessels, brain slices were processed similarly using the above protocol, however, no antigen retrieval was performed, and primary antibody incubation was overnight. The primary antibodies used were rabbit monoclonal antibody against amyloid-beta [mOC64] (1:1000, abcam, catalog# ab201060) and goat polyclonal antibody against alpha-smooth muscle actin (1:500, ThermoFisher Scientific, catalog# PA5-18292). The slices are then washed in PBS and incubated in a secondary antibody solution consisting of donkey anti-goat Alexa Fluor 594 (1:500, Jackson ImmunoResearch) and donkey anti-rabbit Alexa Fluor 488 (1:500, Jackson ImmunoResearch) diluted in a solution of 2% horse serum, 0.1% Triton X-100 in PBS for 2 hours. The sections are washed in PBS and then mounted onto slides for imaging.

For A $\beta$ -pE3 and thioflavin-T co-labeling, 50  $\mu$ m coronal sections underwent the similar treatments as mentioned for the thioflavin-T staining. However, after the final PBS wash step, the sections were incubated with a rabbit polyclonal antibody against A $\beta$ -pE3 (1:1000, Synaptic Systems, Göttingen, Germany, catalog# 218 003) overnight. After the primary antibody incubation, the section was washed with PBS and then incubated with the donkey anti-rabbit Alexa Fluor 405 (1:500, Jackson ImmunoResearch) secondary antibody diluted in 2% horse serum, 0.1% Triton X-100 in PBS for 2 hours. After the secondary antibody incubation, the section was washed with PBS and mounted onto a slide.

For A $\beta$ -pE3 and A $\beta$  co-labeling, 50  $\mu$ m coronal sections were incubated in 99% formic acid for 15 minutes, followed by antigen retrieval using 10 mM Tris-sodium citrate pH 6.0 at 100°C for 5 minutes, cooled for 2 minutes, and then heated again for 5 minutes<sup>99</sup>. The sections were then cooled for about 20 minutes and washed 3 times prior to undergoing the treatments mentioned above except the formic acid treatment, which was already performed. This pre-treatment allowed for better visualization of the A $\beta$  antibody used for this specific set of experiments. Without pre-treatment, the signal is very poor, preventing quantification of A $\beta$  plaques (data not shown). After the blocking step, the sections were incubated

overnight with a rabbit polyclonal antibody against A $\beta$ -pE3 (1:1000, Synaptic Systems, Göttingen, Germany, catalog# 218 003) and a chicken polyclonal antibody against amyloid- $\beta$  (1:250, abcam, catalog# ab134022) diluted in the 5% horse serum, 0.1% Triton X-100 in PBS blocking solution. After the primary antibody incubation, the sections were washed with PBS and then incubated with the donkey anti-rabbit Alex Fluor 488 (1:500, Jackson ImmunoResearch) and donkey anti-chicken Alex Fluor 594 (1:500, Jackson ImmunoResearch) diluted in 2% horse serum, 0.1% Triton X-100 in PBS for 2 hours. After the secondary antibody incubation, the sections were washed with PBS and mounted onto slides.

### ***Image Analysis***

For the A $\beta$  plaque counting, image panels were acquired and stitched using SoftWoRx v1.2 (Applied Science) on a DeltaVision Core system (GE Healthcare Biosciences, Piscataway, NJ) consisting of an Olympus IX71 microscope equipped with a CoolSNAP HQ2 camera (Teledyne Photometrics, Tucson, AZ) on the 10x objective. Each field of view is 1040 x 1040 pixels. For quantification of the microvasculature and microvascular CAA, images were acquired using confocal spinning disk microscopy using the  $\mu$ Manager software on a Leica DM6B microscope equipped with an Evolve Delta camera (Teledyne Photometrics) using a water-immersion 40x objective. Each field of view is 512 x 512 pixels. For data acquisition using confocal microscopy, 10-12 random fields of views from different regions of the brain slice were imaged.

A $\beta$  plaques were manually counted from regions of interest, which were the cerebral cortex and hippocampus for each hemisphere of the mouse brain. The total area of the region of interest is then measured using ImageJ. The plaque numbers are then divided by the area of their corresponding regions of interest to obtain the plaque density. Measurements of percent of A $\beta$ -pE3-positive A $\beta$  plaques was done in a similar manner. The number of A $\beta$ -pE3-positive A $\beta$  plaques was manually counted and then divided by the number of A $\beta$  plaques to obtain a percentage. The number of plaques that are only immunoreactive to

the A $\beta$ -pE3, but not A $\beta$  antibody were also counted to obtain plaque density and percent of A $\beta$ -pE3 plaques that do not co-localize with A $\beta$  plaques.

Data for percentage of the brain area covered in A $\beta$  plaques is obtained by taking the stitched images and subtracting their background using a rolling ball radius of 20 in ImageJ. The images were then subjected to automatic thresholding<sup>100</sup>. The regions of interest are then traced, and the area of the signal within that region was then measured. The area of the signal is then divided by the total area of the region of interest to obtain the percent coverage.

Data for the relative collagen IV volume was obtained from Z-stacks obtained via spinning disk confocal microscopy. The Z-step used was 0.3 $\mu$ m. A background subtraction using rolling ball radius of 100 was applied to each stack, as a rolling ball radius of 20 subtracted a substantial percentage of the signal. We experimented with different values and determined that 100 as an appropriate rolling ball radius as it subtracted out enough of the background without significantly affecting the collagen IV positive signal. The collagen IV stacks were automatically thresholded using the Triangle method.<sup>101</sup> The area of collagen IV positive signal was measured for each image in the stack. The area is then calculated for each image in the stack. The areas are then summed and multiplied by the total number of images in each Z-stack multiplied by the Z-step of 0.3 $\mu$ m to get a volume. This value for collagen IV volume is then divided by the total volume of the Z-stack which is the total area of each stack multiplied by the total number of Z-stacks multiplied by 0.3 $\mu$ m. The resulting value was multiplied by 100 to obtain a percentage value that is referred to as the relative collagen IV volume. For each animal, the percentages from each of the 10-12 regions was averaged to yield a single value.

Measurements for A $\beta$ -pE3 follow the same procedure as above but using the Intermoded thresholding method<sup>102</sup>. We found that thresholding using the Triangle method, as used for the collagen IV, yielded an unsatisfactory representation of the A $\beta$ -pE3 signal. We tried different automatic thresholding methods and determined that Intermoded yielded a satisfactory representation. Area of co-occurrence of A $\beta$ -pE3 and collagen IV signal was then estimated using the AND operator of the Image Calculator on

ImageJ. These area values are calculated for each image in the stack. The areas are then summed and multiplied by the Z-step of 0.3 $\mu$ m to get a volume of collagen IV occupied by A $\beta$ -pE3. This total volume is then divided by the total collagen IV volume for the corresponding image stack. The resulting value is multiplied by 100 to obtain a percentage that is referred to as the relative collagen IV volume occupied by A $\beta$ -pE3. For each animal, the percentages from each of the 10-12 regions was averaged to yield a single value.

Measurements on capillary numbers were done on Max Intensity Projections of the collagen IV Z-stacks. Any vessel that is collagen IV positive and less than 6 $\mu$ m in diameter is considered a capillary. Each branch on the blood vessel that meets this criterion is counted as a capillary. Thus, when a vessel branches into two vessels, that original vessel along with its two branches would be counted as three separate vessels. The capillaries per field of view are then manually counted.

Data for CAA in the pial vessels is obtained on stitched images of the entire brain slice immunolabeled for  $\alpha$ -smooth muscle actin and A $\beta$ . The number of  $\alpha$ -smooth muscle actin-positive vessels on the brain surface is manually counted. Structures that display positive labeling and possess a lumen as counted as vessel and nearby features are considered so that the same vessel is not counted multiple times. The A $\beta$  signal is then overlaid with the  $\alpha$ -smooth muscle actin signal and the number of vessels that exhibit A $\beta$  accumulation is also then manually counted. For each mouse, the number of A $\beta$ - and  $\alpha$ -smooth muscle actin-positive pial vessels was divided by the total number of pial vessels to obtain a percentage, which is termed percent pial vessels displaying CAA.

### ***Statistical Analysis***

All statistical tests were performed with GraphPad Prism v9.0. Data are expressed as means  $\pm$  SEM. Each data point represents a single mouse. Measurements of thioflavin-T and A $\beta$ -pE3 plaque density are analyzed using two-tailed Mann Whitney test. A non-parametric Mann Whitney test was used for these data

because statistical analysis suggested that the plaque density values did not follow a normal distribution. The remaining measurements such as plaque density of A $\beta$ -pE3-positive A $\beta$  plaques, percent of A $\beta$  plaques that are A $\beta$ -pE3-positive, plaque density of A $\beta$ -pE3 only plaques, percent of A $\beta$ -pE3 only plaques, A $\beta$ -mOC64 plaque density, plaque coverage, relative collagen IV volume, capillary counts, and CAA are analyzed using two-tailed *Student's* T-test as data followed a Gaussian distribution. All data are expressed as means  $\pm$  SEM. A p-value smaller than 0.05 ( $p < 0.05$ ) is considered significant.

## **Results**

### ***No sex differences observed in thioflavin-T plaque density***

Labeling 3-month-old *5x-FAD* mice with thioflavin-T revealed plaque accumulation in several brain regions, notably the cortex and hippocampus (**Figure 2B, D**). As expected, no thioflavin-T reactive plaques were observed in brain slices from age-matched wild-type mice (**Figure 2A, C**). Despite a seemingly higher number of thioflavin-T plaques in the cortex (**Figure 3A, B**) and hippocampus (**Figure 4A, B**) of female *5x-FAD*, these apparent sex differences were not statistically significant when data were analyzed in an unbiased manner (**Figure 3C, D and 4C, D**). In the cortex, there is no statistically significant difference in plaque density ( $26.83 \pm 4.83$  vs  $69.83 \pm 21.82$ , males vs. females,  $p = 0.054$ ) (**Figure 3C**) or plaque coverage ( $0.31 \pm 0.04$  vs  $0.49 \pm 0.13$ , males vs. females,  $p = 0.2051$ ) (**Figure 3D**). Similarly, in the hippocampus, there is no statistically significant sex difference in the plaque density ( $17.67 \pm 2.10$  vs  $59.76 \pm 22.01$ , males vs. females,  $p = 0.189$ ) (**Figure 4C**) or plaque coverage ( $0.45 \pm 0.08$  vs  $0.61 \pm 0.17$ , males vs. females,  $p = 0.379$ ) (**Figure 4D**).

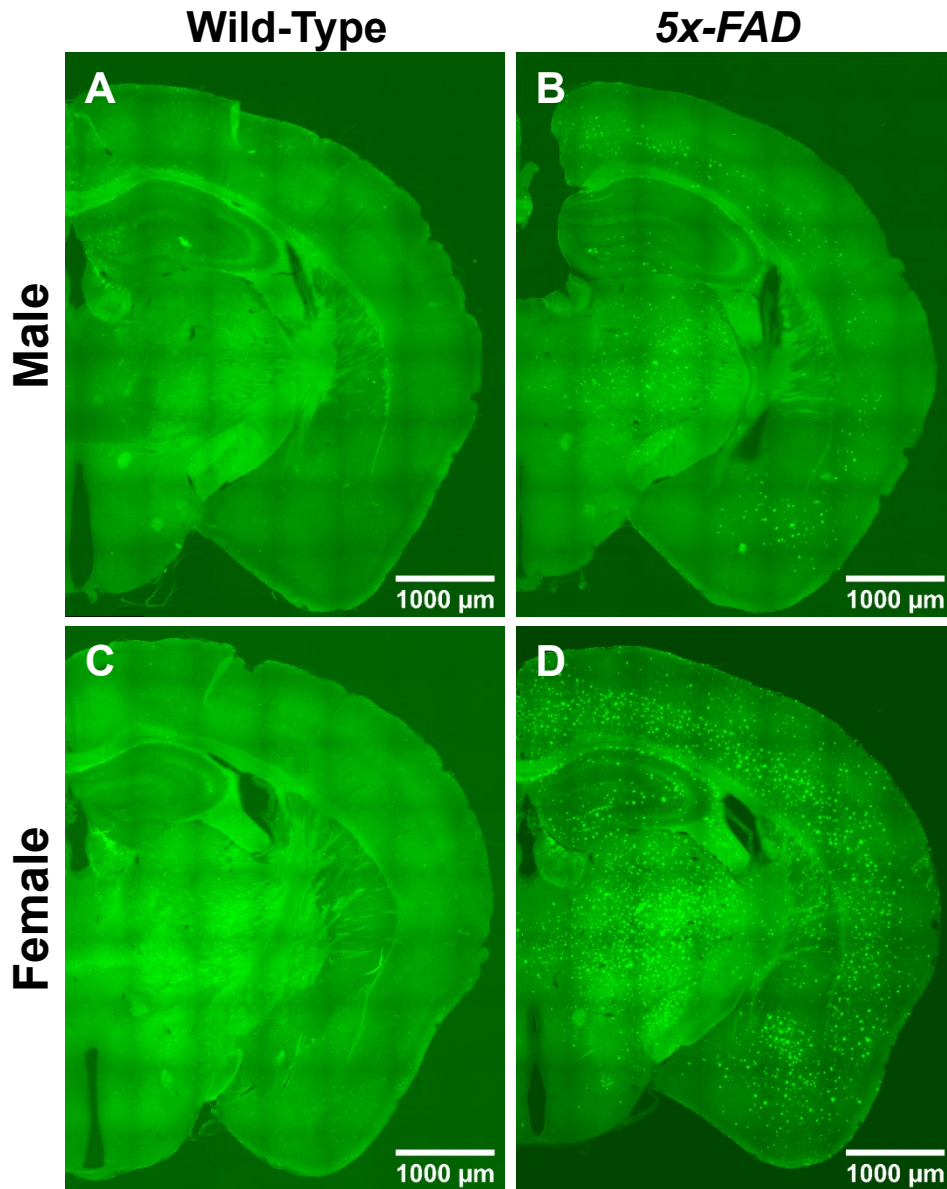


**Figure 2.** *Thioflavin-T Staining of mouse brain slices.* 3-month-old male (A) and female (C) wild-type mice of both sexes display no thioflavin-T-reactive A $\beta$  plaques compared to male (B) and female (D) *5x-FAD* mice.

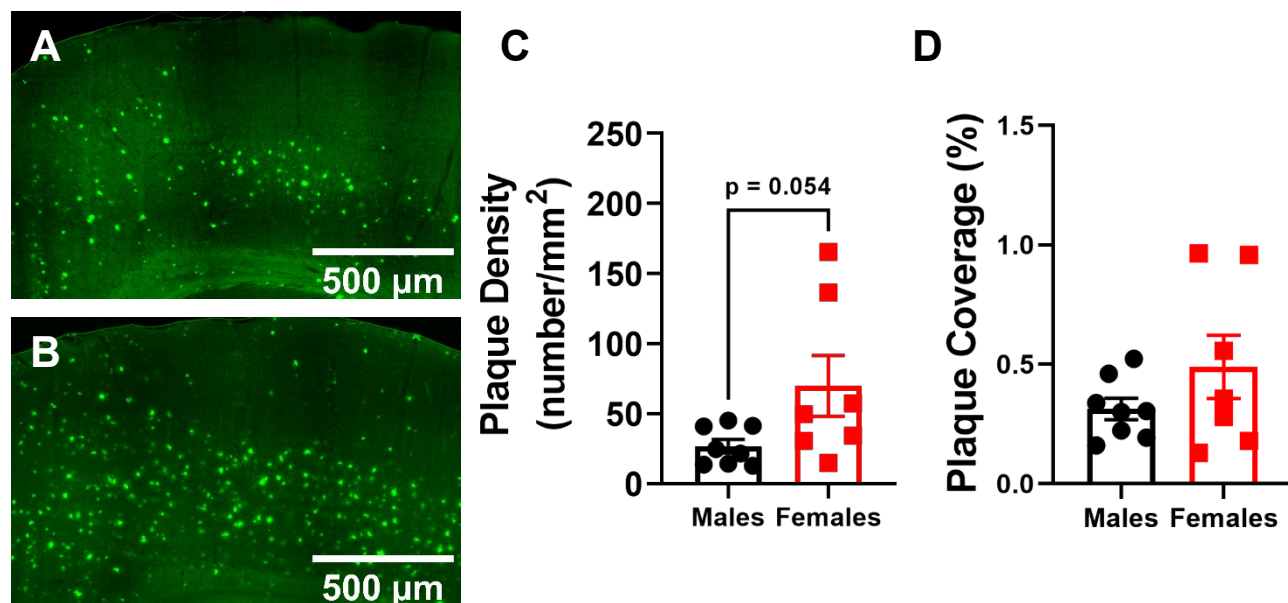


**Figure 3.** Thioflavin-T plaque density in cortex of 3-month-old 5x-FAD mice. Thioflavin-T reactive Aβ plaques are present in the cortex of male (A) and female (B) 5x-FAD mice. The data are represented as plaque density (C) or plaque coverage (D). Data are expressed as means ± SEM. Two-tailed Mann Whitney test for the plaque density or two-tailed *Student's* T-Test for the plaque coverage.

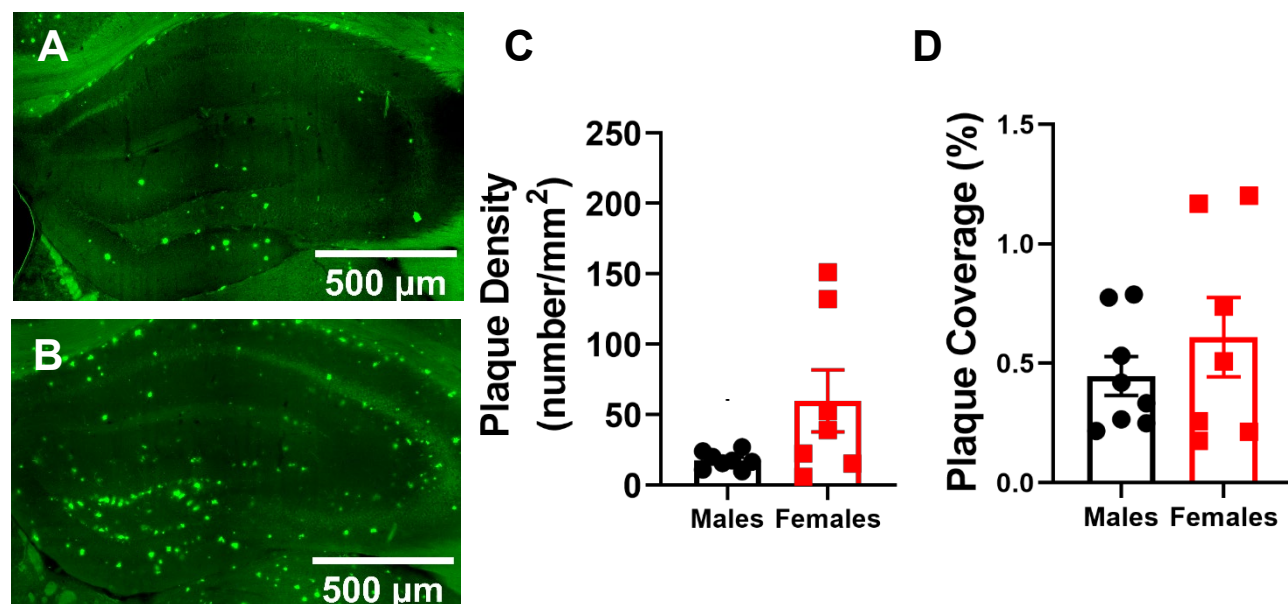


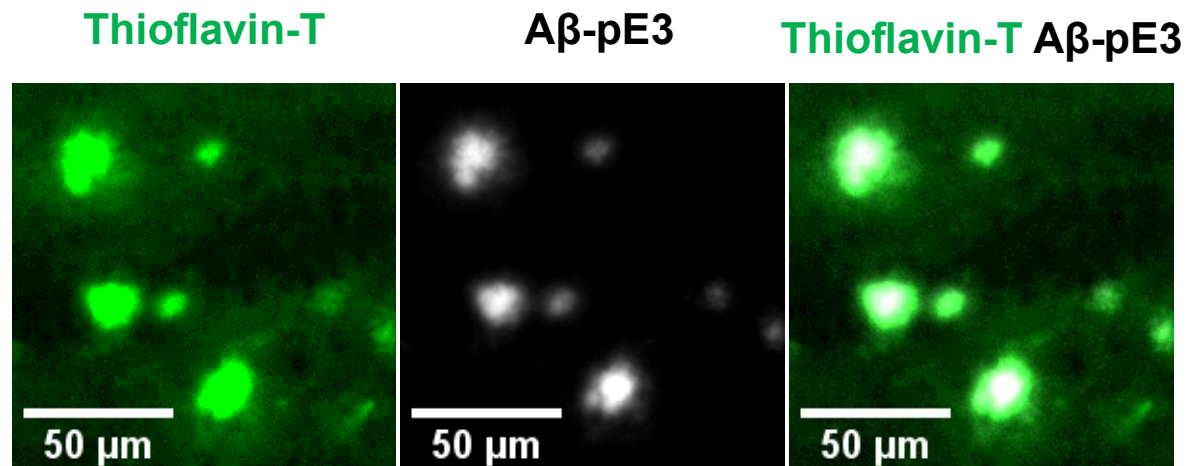
**Figure 4.** Thioflavin-T plaque density in hippocampus of 3-month-old 5x-FAD mice. Thioflavin-T reactive Aβ plaques are present in the hippocampus of male (A) and female (B) 5x-FAD mice. The data are

represented as plaque density (C) or plaque coverage (D). Data are expressed as means  $\pm$  SEM. Two-tailed Mann Whitney test for the plaque density or two-tailed *Student's* T-Test for the plaque coverage.

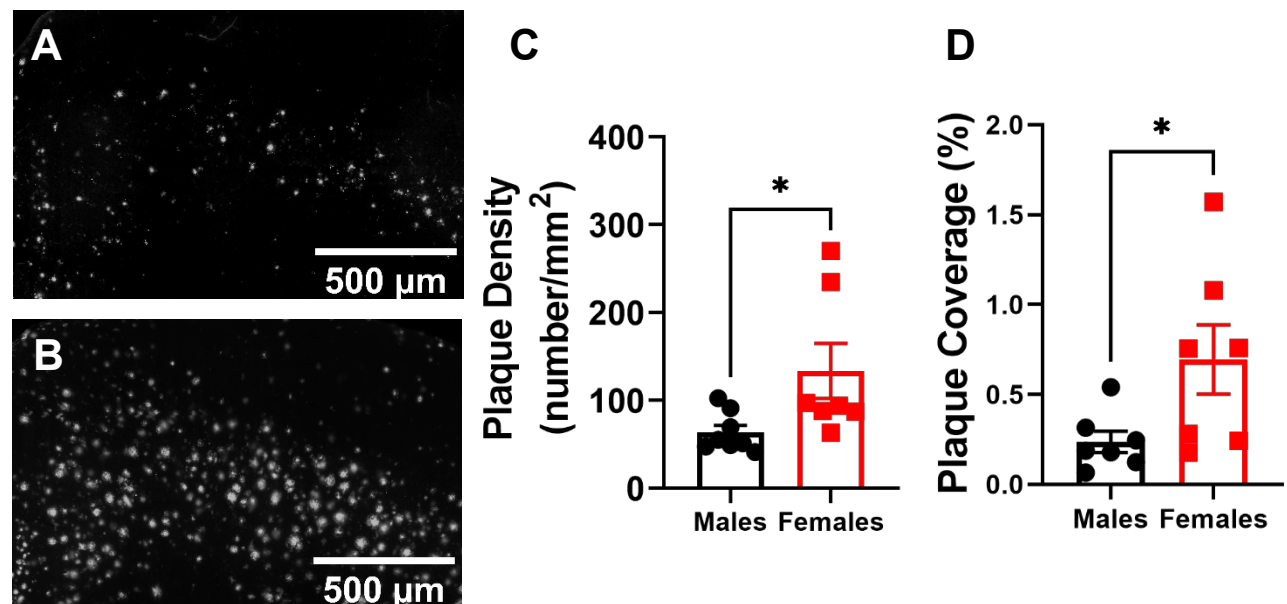
### ***Higher A $\beta$ -pE3 parenchymal plaque burden in female 5x-FAD***

Immunostaining for A $\beta$ -pE3 revealed a similar pattern of localization as thioflavin-T. As expected, A $\beta$ -pE3-positive plaques are in the core of the thioflavin-T plaques (**Figure 5**). Also, A $\beta$ -pE3 are present throughout the cortex (**Figure 6A, B**) and hippocampus (**Figure 7A, B**) in 5x-FAD mice. In contrast to thioflavin-T staining, A $\beta$ -pE3 plaque density and coverage were significantly greater in the cortex (**Figure 6C, D**) and hippocampus (**Figure 7C, D**) of females 5x-FAD when compared to males. In the cortex, there is a statistically significant difference in A $\beta$ -pE3 plaque density ( $63.45 \pm 7.89$  vs  $133.40 \pm 31.25$ , males vs. females,  $p = 0.029$ ) (**Figure 6C**) and plaque coverage ( $0.237 \pm 0.06$  vs  $0.70 \pm 0.19$ , males vs. females,  $p = 0.043$ ) (**Figure 6D**). Similarly, in the hippocampus, there is a statistically significant difference in plaque density ( $35.64 \pm 7.26$  vs  $89.92 \pm 23.31$ , males vs. females,  $p = 0.029$ ) (**Figure 7C**) and plaque coverage ( $0.15 \pm 0.03$  vs  $0.43 \pm 0.12$ , males vs. females,  $p = 0.038$ ) (**Figure 7D**). Co-labeling the brains with an A $\beta$  antibody revealed that A $\beta$ -pE3 is present in some of these plaques (**Figure 8A, Figure 9A**). Quantification of the number of A $\beta$  plaques that are positive for A $\beta$ -pE3 revealed no sex differences in density of these plaques in either the cortex ( $26.76 \pm 7.23$  vs  $89.83 \pm 29.54$ , males vs. females,  $p = 0.065$ ) (**Figure 8B**) or the hippocampus ( $18.12 \pm 4.14$  vs  $53.98 \pm 28.93$ , males vs. females,  $p = 0.248$ ) (**Figure 9B**). However, the percent of A $\beta$  plaques that are positive for A $\beta$ -pE3 is significantly greater in 5x-FAD females compared to males in the cortex ( $36.60 \pm 4.65$  vs  $66.10 \pm 7.96$ , males vs. females,  $p = 0.010$ ) (**Figure 8C**) and hippocampus ( $44.26 \pm 4.63$  vs  $63.09 \pm 6.85$ , males vs. females,  $p = 0.046$ ) (**Figure 9C**). It was also noted that there were some plaques that were positive only for A $\beta$ -pE3, but not A $\beta$ . There were no observed sex differences in the density of these plaques in the cortex ( $22.65 \pm 6.43$  vs  $56.18 \pm 31.88$ , males vs. females,  $p = 0.327$ ) (**Figure 8D**) or hippocampus ( $14.97 \pm 3.63$  vs  $45.99 \pm 34.85$ , males vs. females,  $p = 0.397$ ) (**Figure 9D**). Quantification of these plaques revealed that they comprise approximately 30-50% of A $\beta$ -

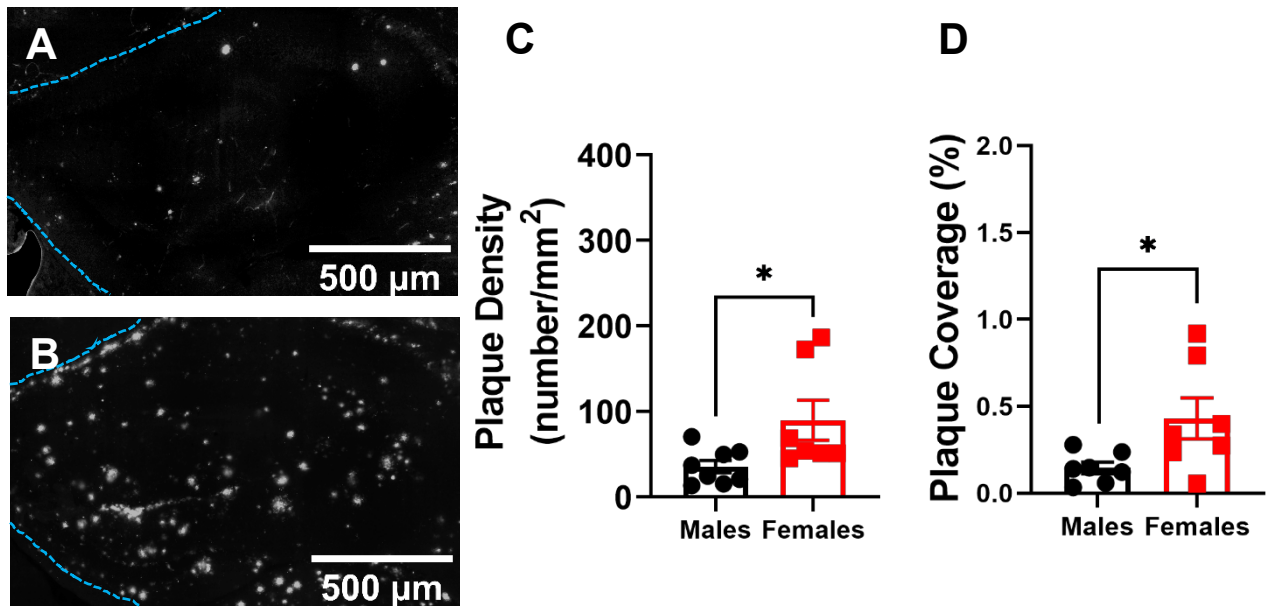
pE3 plaques in the cortex ( $37.33 \pm 4.39$  vs  $30.58 \pm 6.08$ , males vs. females,  $p = 0.389$ ) (**Figure 8E**) and hippocampus ( $44.26 \pm 4.63$  vs  $41.55 \pm 8.19$ , males vs. females,  $p = 0.779$ ) (**Figure 9E**) without sex differences.



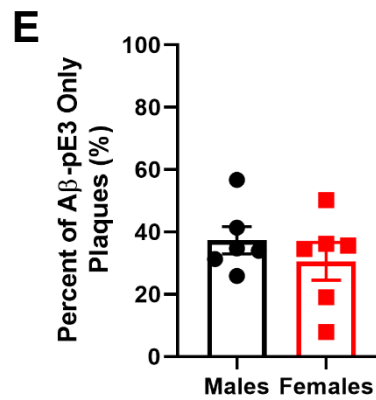
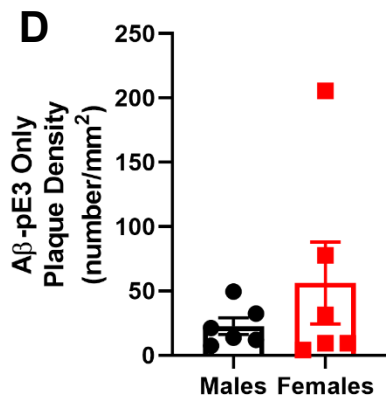
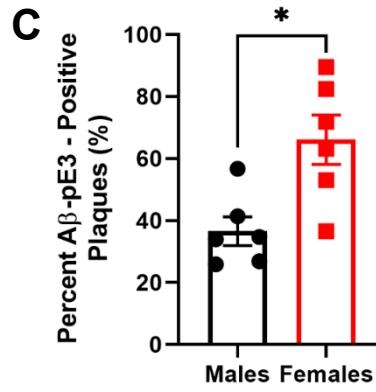
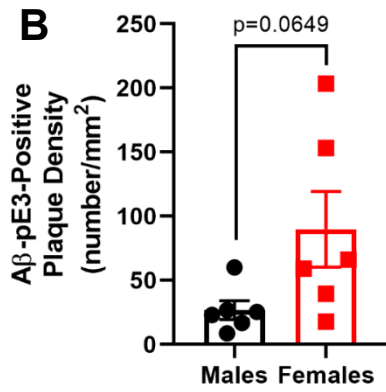
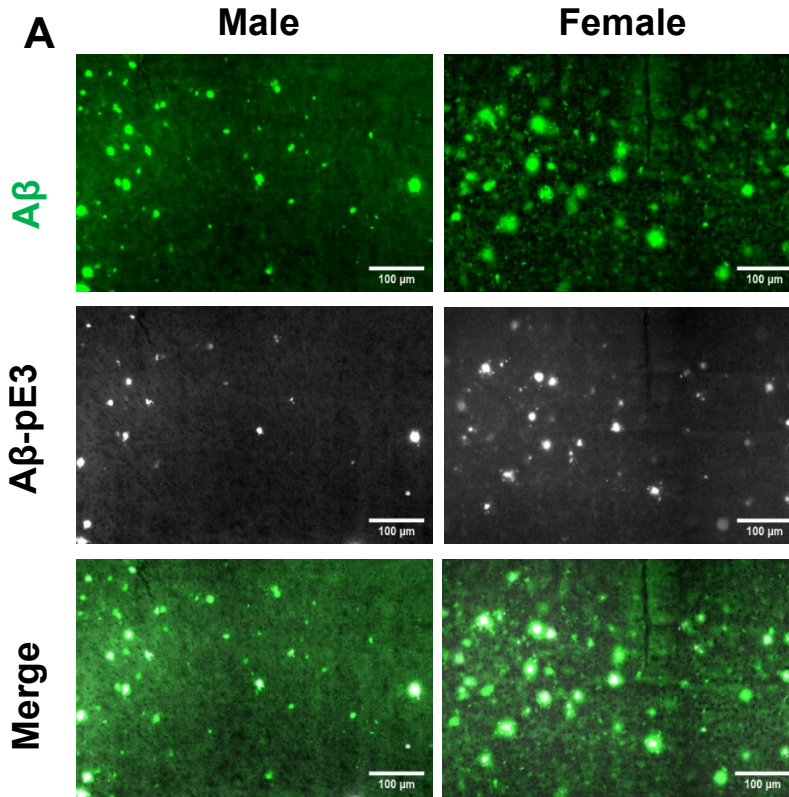
**Figure 5.** *Aβ-pE3* is localized to the core of *Aβ* plaques. *Aβ-pE3*-positive plaques shown in grey seem to be in the core of thioflavin-T-positive plaques shown in green.



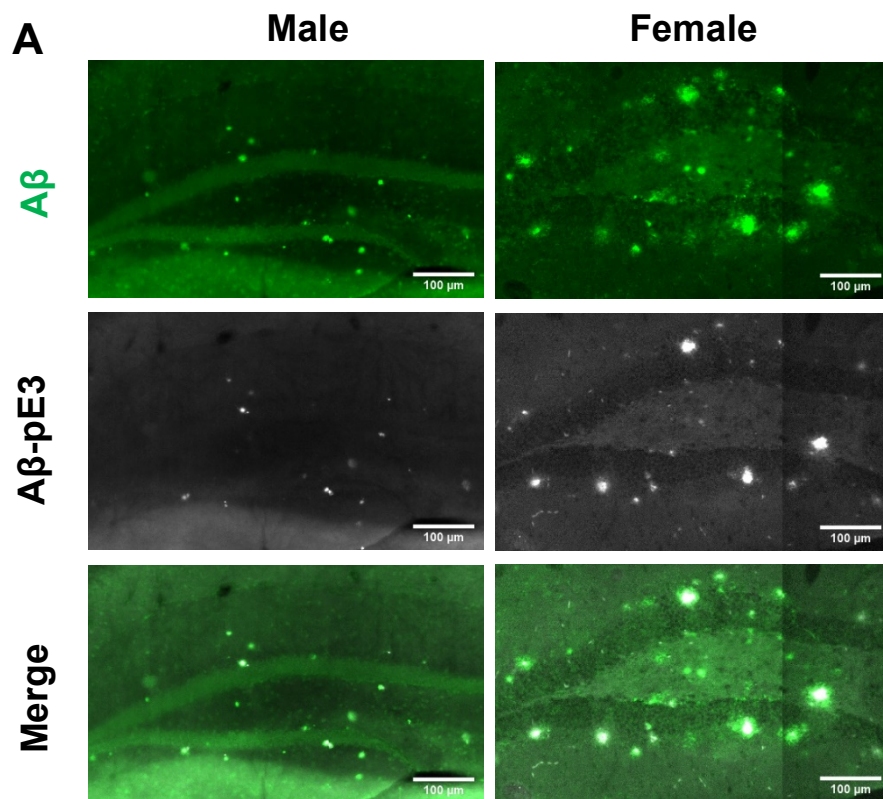
**Figure 6.** *Aβ-pE3* plaque density in cortex of 3-month-old *5x-FAD* mice. Aβ-pE3 reactive Aβ plaques are present in the cortex of male (A) and female (B) *5x-FAD* mice. The data are represented as plaque density (C) or plaque coverage (D). Data are expressed as means ± SEM. \*  $p < 0.05$ , two-tailed Mann Whitney test or two-tailed *Student's* T-Test for the plaque coverage.



**Figure 7.** *Aβ-pE3* plaque density in the hippocampus of 3-month-old *5x-FAD* mice. Aβ-pE3 reactive Aβ plaques are present in the hippocampus of male (A) and female (B) *5x-FAD* mice. Blue dotted lines delineate the edges of the hippocampus. The data are represented as plaque density (C) or plaque coverage (D). Data are expressed as means ± SEM. \*  $p < 0.05$ , two-tailed Mann Whitney test or two-tailed *Student's* T-Test for the plaque coverage.



**Figure 8.** Density and percent of A $\beta$  plaques positive for A $\beta$ -pE3 in the cortex of 3-month-old 5x-FAD mice. A $\beta$ -pE3, shown in white, is localized to the core of some A $\beta$  plaques, shown in green, in the cortex of male and female 5x-FAD mice (A). The data are represented as plaque density (B) or percent of A $\beta$  plaques that are also positive for A $\beta$ -pE3 (C). Additionally, there are some plaques comprised of A $\beta$ -pE3, but not A $\beta$ , referred to here as A $\beta$ -pE3 only plaques. The data are represented as plaque density (D) and percent of A $\beta$ -pE3 plaques that are not co-localized with general A $\beta$  plaques (E). Data are expressed as means  $\pm$  SEM. \*  $p < 0.05$ , two-tailed *Student's* T-test.



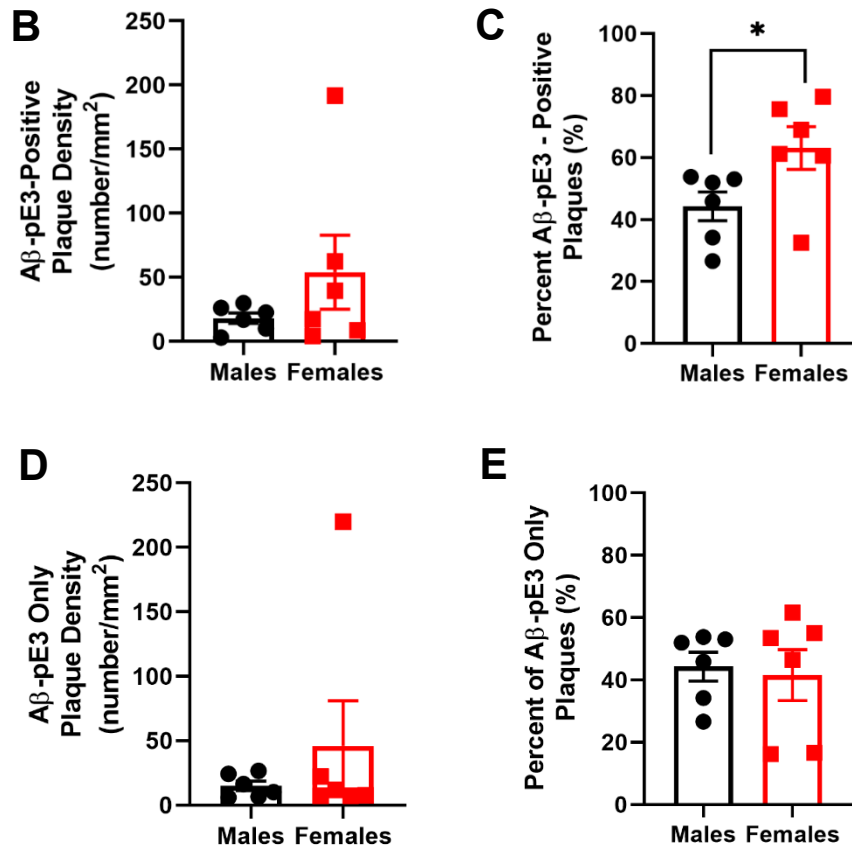
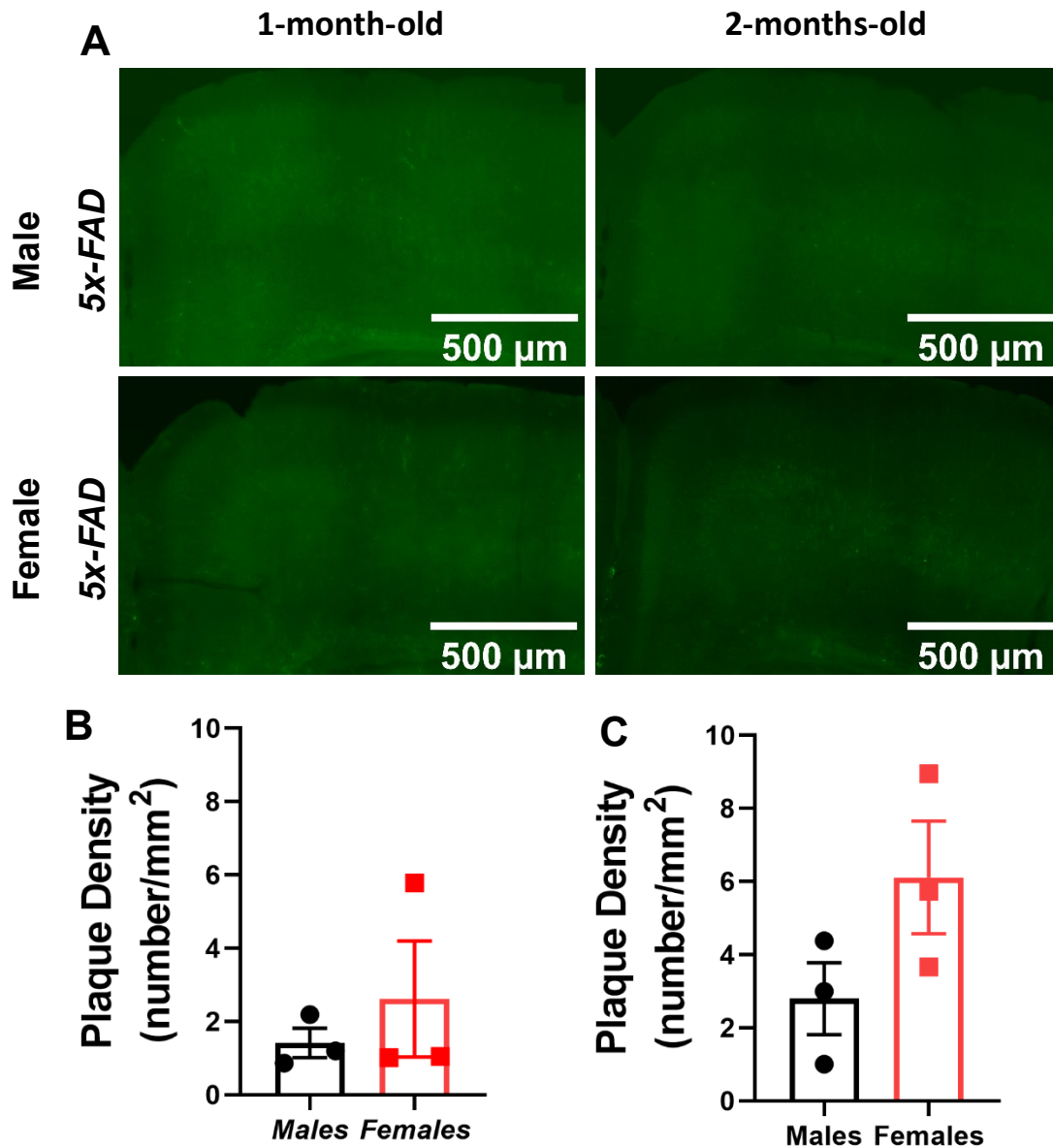


**Figure 9.** Density and percent of A $\beta$  plaques positive for A $\beta$ -pE3 in the hippocampus of 3-month-old 5x-FAD mice. A $\beta$ -pE3, shown in white, is localized to the core of some A $\beta$  plaques, shown in green, in the hippocampus of male and female 5x-FAD mice (A). The data are represented as plaque density (B) or percent of A $\beta$  plaques that are also positive for A $\beta$ -pE3 (C). Additionally, there are some plaques comprised of A $\beta$ -pE3, but not A $\beta$ , referred to here as A $\beta$ -pE3 only plaques. The data are represented as plaque density (D) and percent of A $\beta$ -pE3 plaques that are not co-localized with general A $\beta$  plaques (E). Data are expressed as means  $\pm$  SEM. \*  $p < 0.05$ , two-tailed *Student's* T-test.

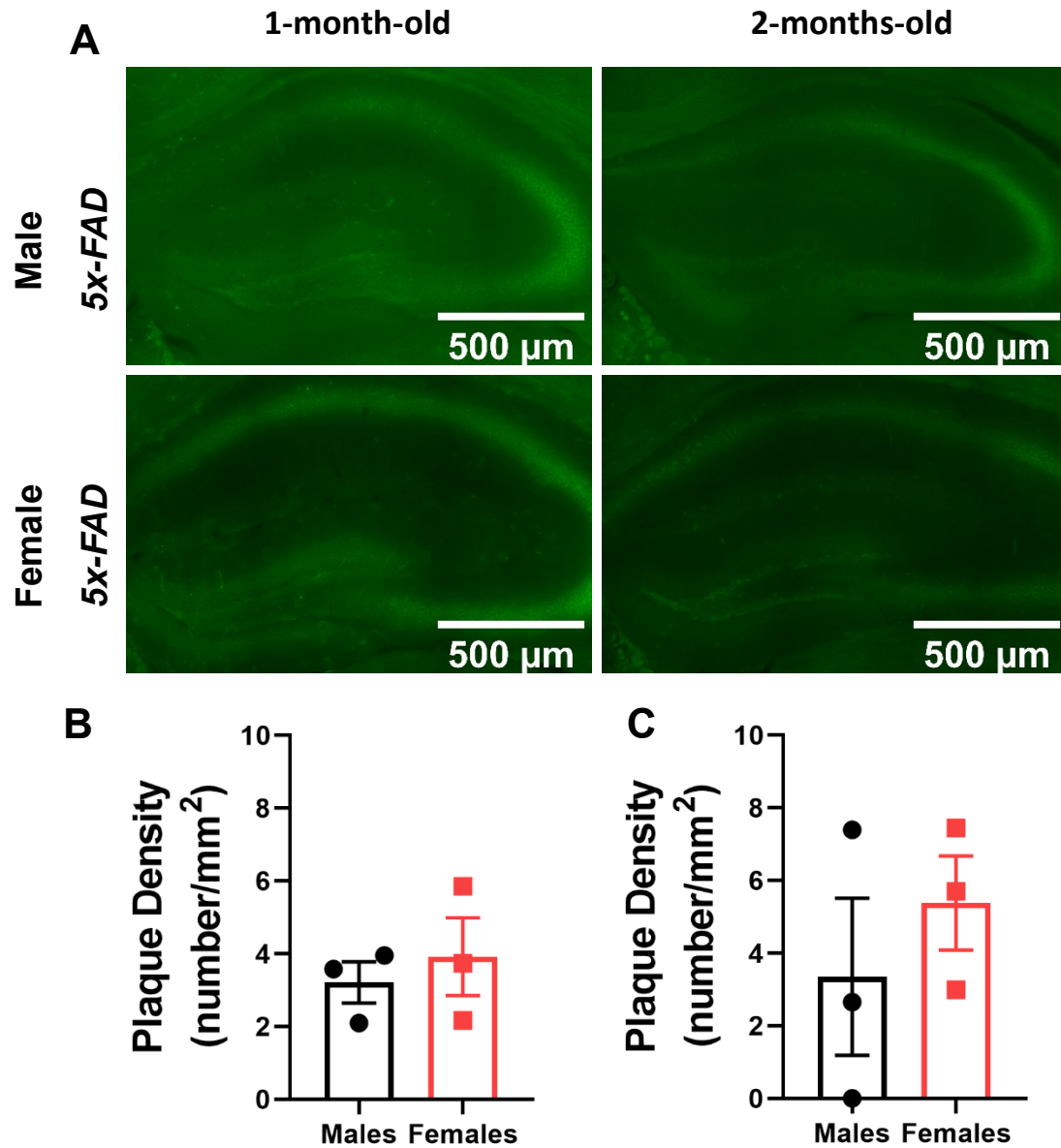
### *A $\beta$ and A $\beta$ -pE3 plaques accumulate in 5x-FAD mice at 2 months of age*

A pilot study looking at plaque accumulation in the cortex and hippocampus of 1- and 2-month-old 5x-FAD male and female mice using thioflavin-T (Figure 10, Figure 11), an antibody against A $\beta$ -mOC64

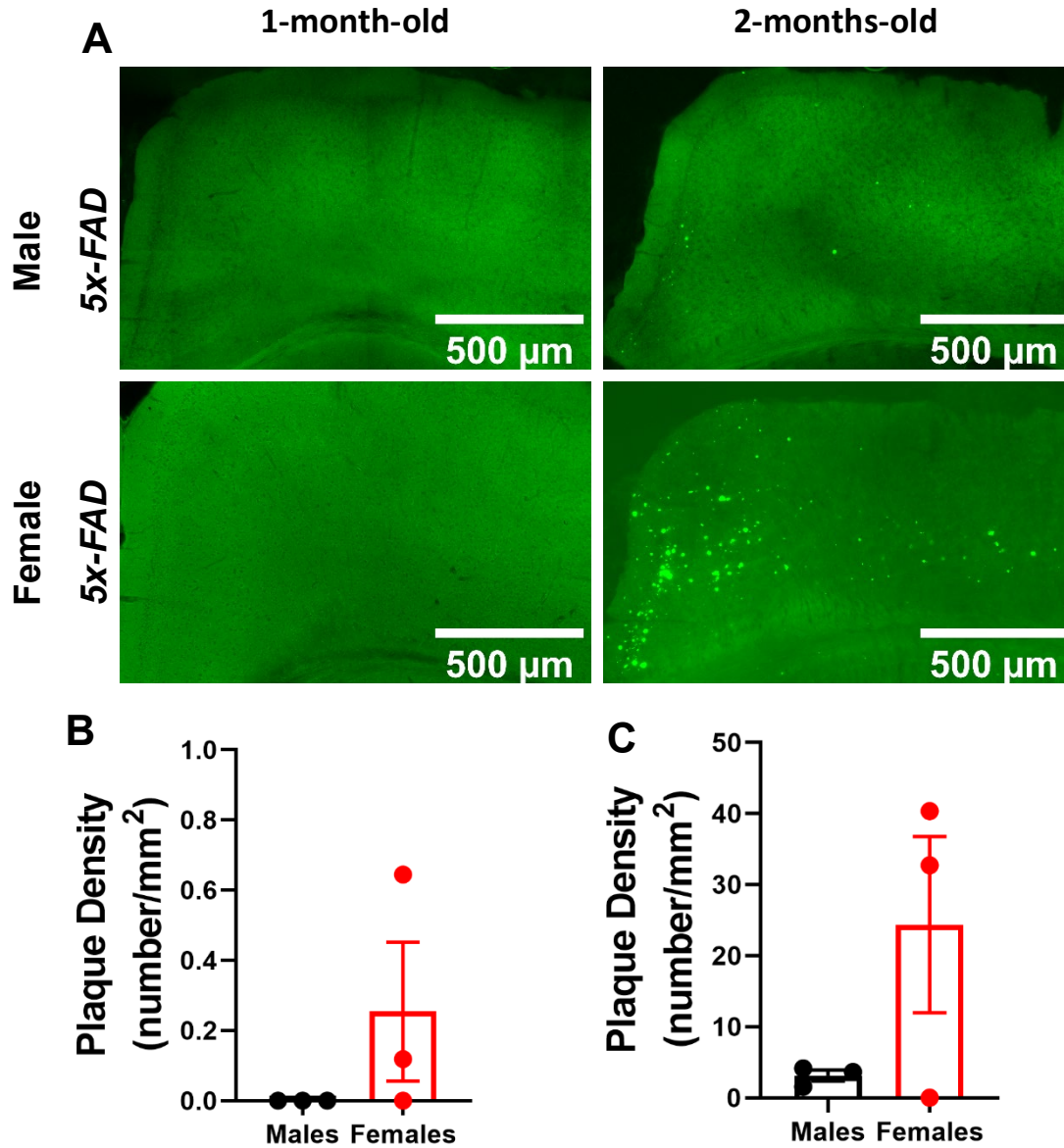
(**Figure 12, Figure 13**), or an antibody against A $\beta$ -pE3 (**Figure 14, Figure 15**) suggests no sex differences in overall A $\beta$  or A $\beta$ -pE3 accumulation in 1- or 2-month-old *5x-FAD* mice. Using Thioflavin-T, no sex differences were observed in these mice at 1 month of age in either the cortex ( $1.42 \pm 0.40$  vs  $2.61 \pm 1.58$ , males vs. females,  $p = 0.504$ ) or the hippocampus ( $3.21 \pm 0.57$  vs  $3.92 \pm 1.07$ , males vs. females,  $p = 0.588$ ). Similarly, with the A $\beta$  antibody, no sex differences were observed in these mice at 1 month of age in the cortex ( $0 \pm 0.00$  vs  $0.25 \pm 0.20$ ,  $p = 0.268$ ) or the hippocampus ( $0.02 \pm 0.02$  vs  $0.00 \pm 0.00$ ,  $p = 0.374$ ). At 2 months of age, thioflavin-T staining of the cortex ( $1.42 \pm 0.40$  vs  $2.61 \pm 1.58$ , males vs. females,  $p = 0.504$ ) and hippocampus ( $3.21 \pm 0.57$  vs  $3.92 \pm 1.07$ , males vs. females,  $p = 0.588$ ) also revealed no sex differences. Additionally, no sex differences were observed in the cortex ( $3.12 \pm 0.78$  vs  $24.37 \pm 12.38$ , males versus females,  $p = 0.162$ ) or hippocampus ( $1.17 \pm 0.55$  vs  $5.00 \pm 3.00$ , males vs. females,  $p = 0.278$ ) of the 2-month-old mice with the A $\beta$  antibody. At 1 month of age, *5x-FAD* mice of either sex displayed little A $\beta$  in the cortex and hippocampus as detected by either thioflavin-T (**Figure 10A-B; Figure 11A-B**) or an A $\beta$  antibody (**Figure 12A-B, Figure 13A-B**). However, parenchymal A $\beta$  plaques were present by 2 months of age, primarily in the cortex (**Figure 10A,C; Figure 12A,C**) with few in the hippocampus (**Figure 11A,C; Figure 13A,C**), suggesting that overall A $\beta$  plaque accumulation may begin between 1 or 2 months in this model. Similarly, at 1 month of age, *5x-FAD* mice of either sex displayed little to no A $\beta$ -pE3 plaques in the cortex ( $0.30 \pm 0.19$  vs  $0.16 \pm 0.031$ , males vs. females,  $p = 0.511$ ) (**Figure 14A-B**) or hippocampus ( $0.44 \pm 0.44$  vs  $0.66 \pm 0.19$ , males vs. females,  $p = 0.666$ ) (**Figure 15A-B**). More A $\beta$ -pE3 plaques were present in the cortex ( $0.53 \pm 0.13$  vs  $6.71 \pm 3.48$ , males vs. females,  $p = 0.151$ ) (**Figure 14A,B**) and hippocampus ( $1.47 \pm 0.67$  vs  $4.69 \pm 1.84$ , males vs. females,  $p = 0.175$ ) (**Figure 15A,C**) of 2-month-old *5x-FAD* mice compared to the 1-month-old mice. Although female mice appear to possess a somewhat greater overall A $\beta$  and A $\beta$ -pE3 plaque density, most notably in the cortex (**Figure 10C, Figure 12B, Figure 12C, Figure 14C**), no significance was observed suggesting some variability in the onset of A $\beta$  among these mice. However, due to the relatively small sample size used for these particular studies, it is difficult to draw definitive conclusions.



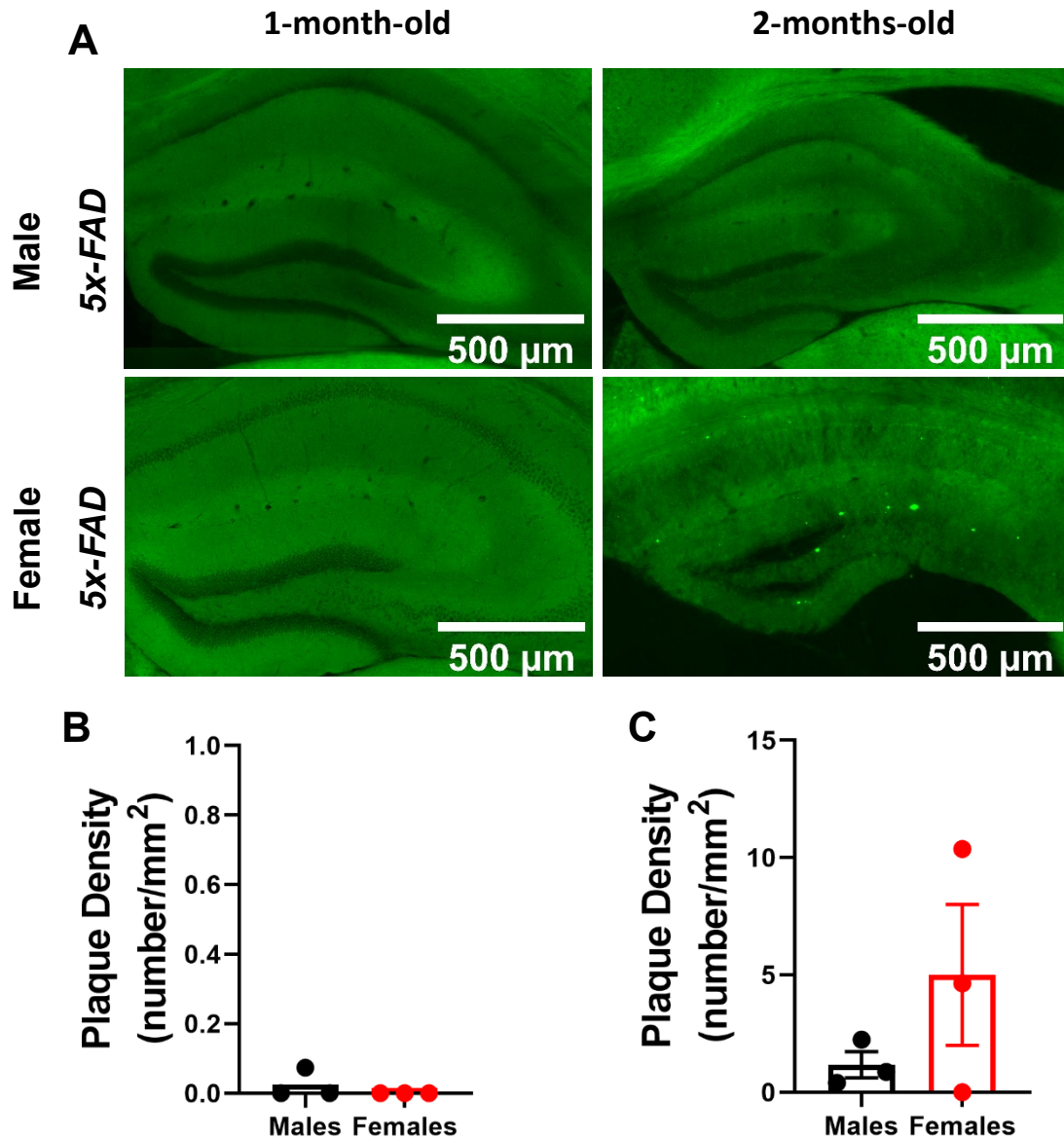
**Figure 10.** 1- and 2-month-old 5x-FAD male and female mice have few thioflavin-T reactive  $A\beta$  plaque accumulation in the cortex. Representative images of thioflavin-T staining from cortex of these mice (A). The data is represented as plaque density for 1-month-old (B) or 2-month-old (C) male and female 5x-FAD mice. Data are expressed as means  $\pm$  SEM. Two-tailed *Student's* T-test.



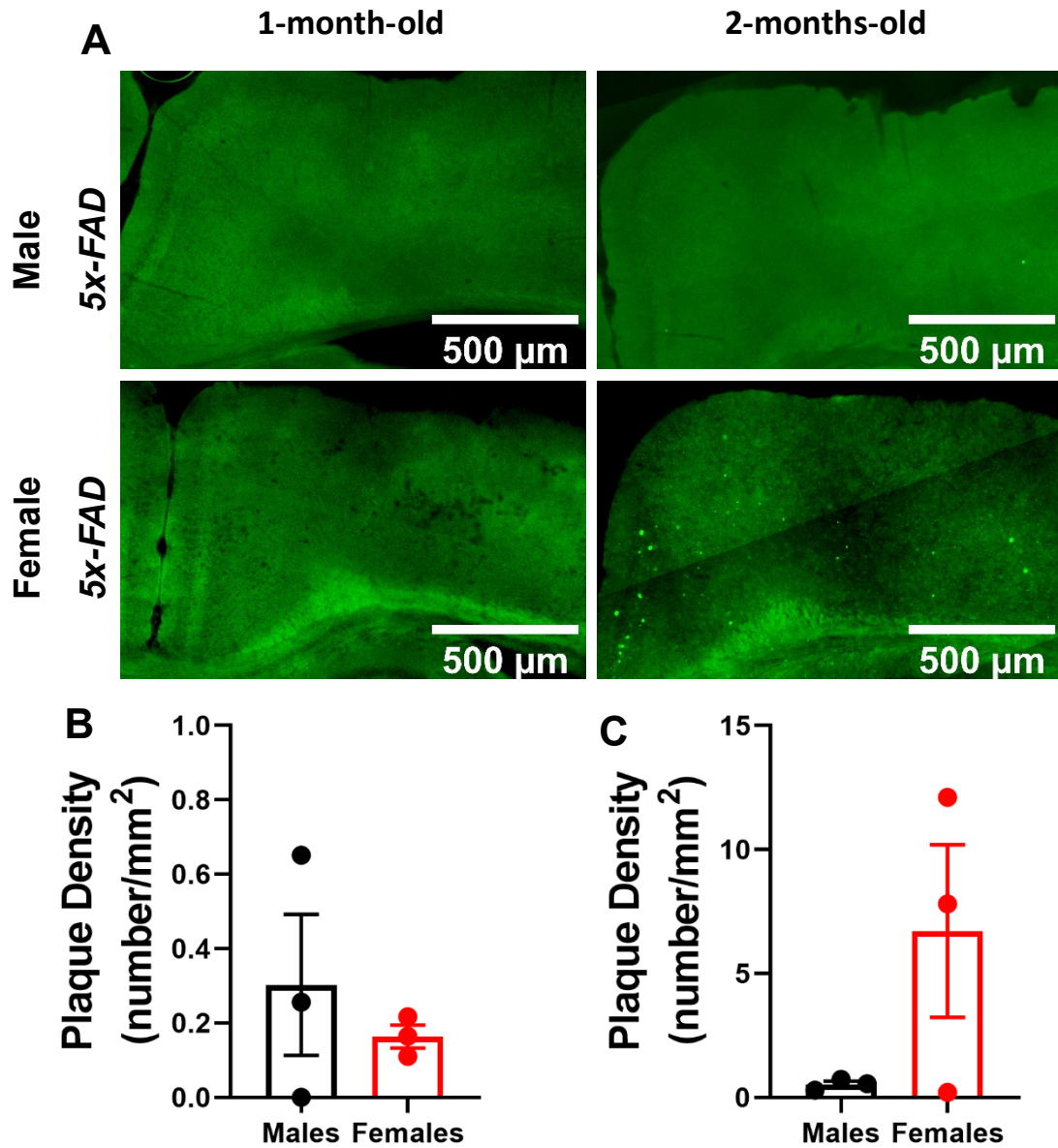
**Figure 11.** 1- and 2-month-old 5x-FAD male and female mice have few thioflavin-T reactive  $A\beta$  plaque accumulation in the hippocampus. Representative images of thioflavin-T staining from cortex of these mice (A). The data is represented as plaque density for 1-month-old (B) or 2-month-old (C) male and female 5x-FAD mice. Data are expressed as means  $\pm$  SEM. Two-tailed *Student's* T-test.



**Figure 12.**  $A\beta$  antibody detects plaques in 2-, but not 1-month old, 5x-FAD male and female in the cortex. Representative images from cortex of these mice labeled with an antibody against  $A\beta$ -mOC64 (A). The data is represented as plaque density for 1-month-old (B) or 2-month-old (C) male and female 5x-FAD mice. Data are expressed as means  $\pm$  SEM. Two-tailed *Student's* T-test.

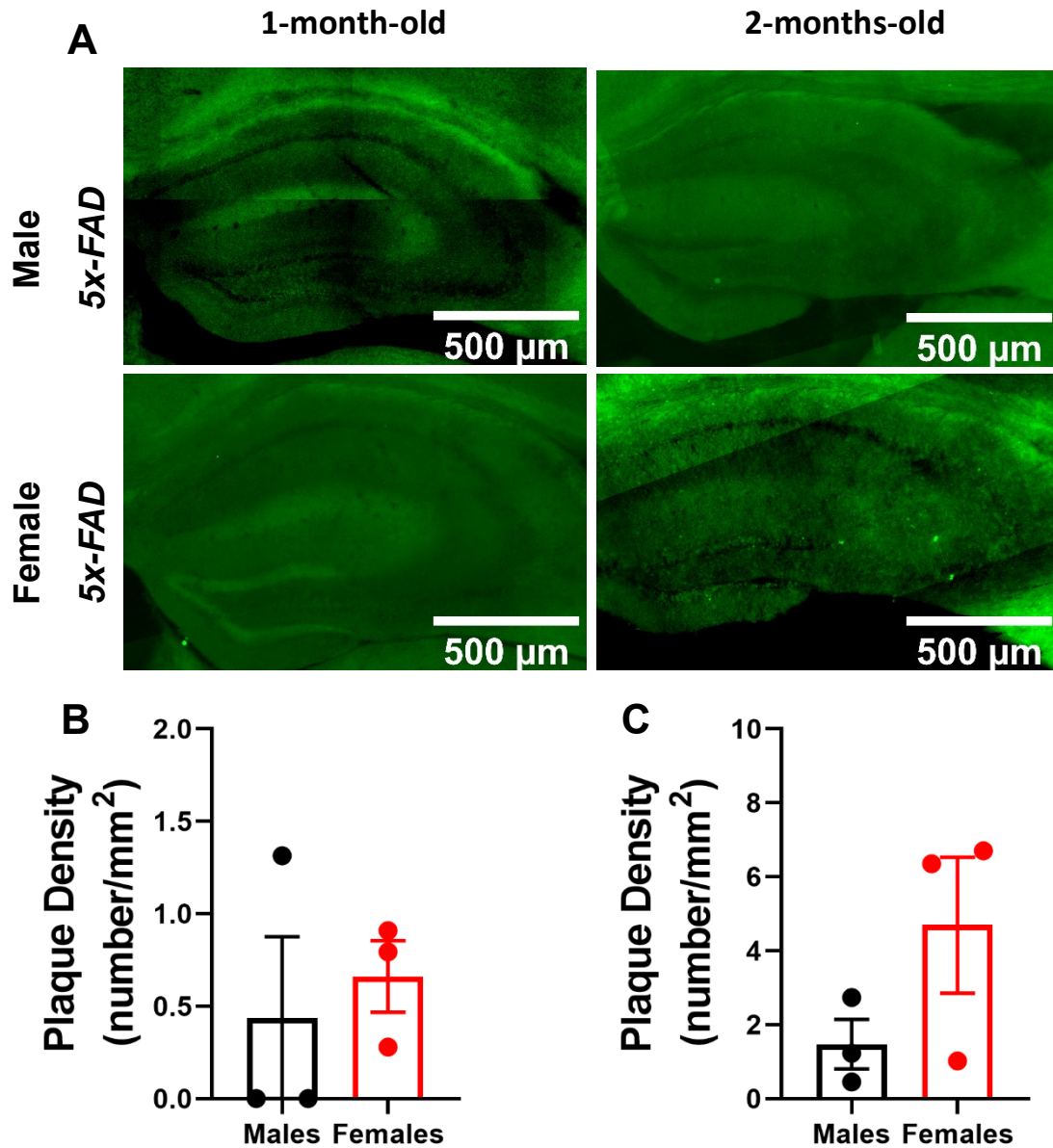


**Figure 13.**  $A\beta$  antibody detects few plaques in 2-, but not 1-month-old, 5x-FAD male and female mice in the hippocampus. Representative images from the hippocampus of these mice labeled with an antibody against  $A\beta$ -mOC64 (A). The data is represented as plaque density or plaques per mm<sup>2</sup> for 1-month-old (B) or 2-month-old (C) male and female 5x-FAD mice. Data are expressed as means  $\pm$  SEM. Two-tailed Student's T-test.



**Figure 14.** *Aβ-pE3* plaques are present in 2-, but not 1-month old, 5x-FAD male and female in the cortex.

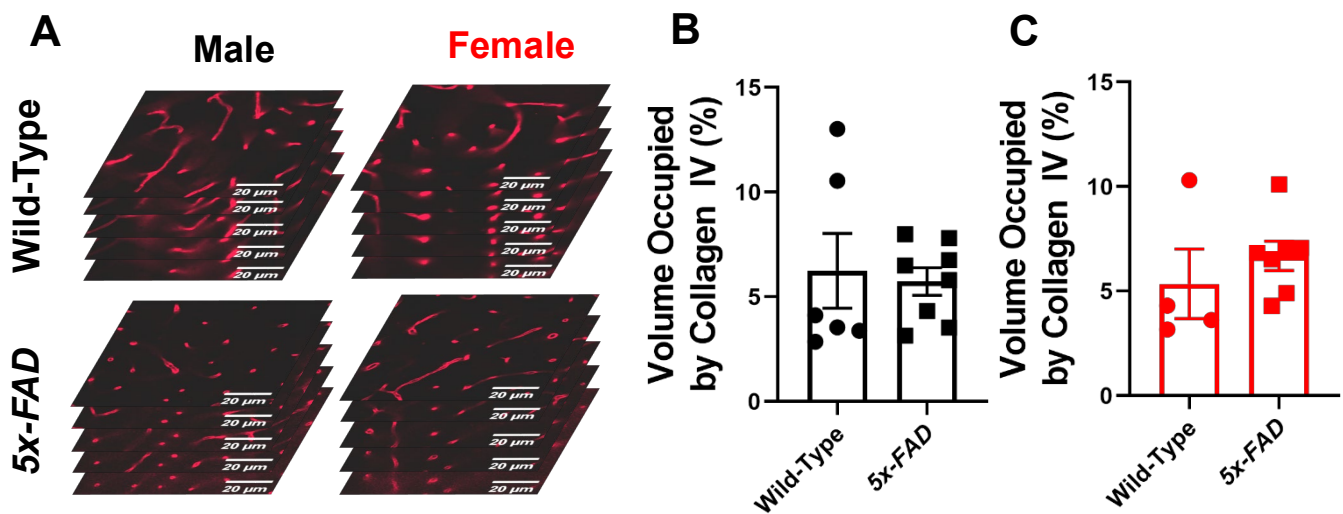
Representative images from cortex of these mice labeled with an antibody against Aβ-pE3 (A). The data is represented as plaque density for 1-month-old (B) or 2-month-old (C) male and female 5x-FAD mice. Data are expressed as means ± SEM. Two-tailed *Student's* T-test.

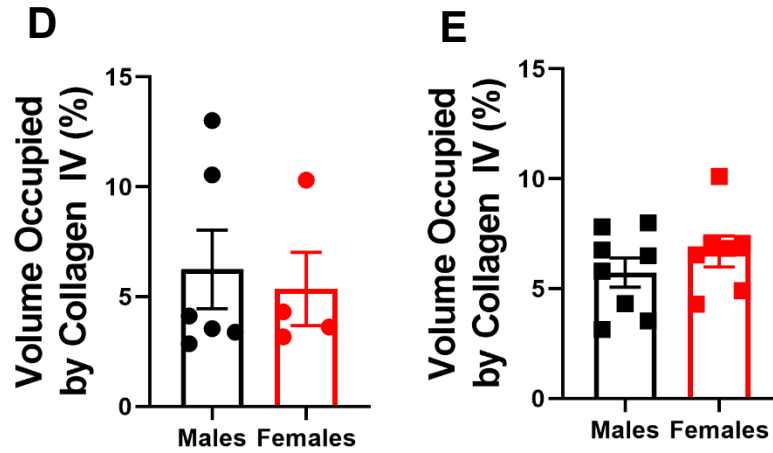


**Figure 15.** Few  $A\beta$ -pE3 plaques are present in 2-, but not 1-month-old, 5x-FAD male and female in the hippocampus. Representative images from cortex of these mice labeled with an antibody against  $A\beta$ -pE3 (A). The data is represented as plaque density for 1-month-old (B) or 2-month-old (C) male and female 5x-FAD mice. Data are expressed as means  $\pm$  SEM. Two-tailed *Student's* T-test.

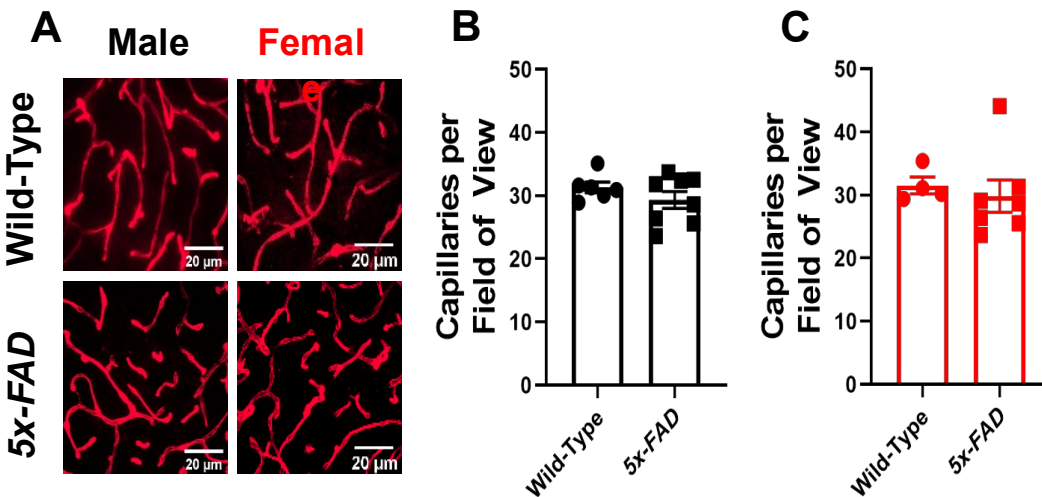
*Capillary numbers are not altered in 5x-FAD mice*

Immunostaining for collagen IV in male and female wild-type and *5x-FAD* mice (**Figure 16A**) showed that there were no significant differences in the relative collagen IV volume between strains (wild-type vs *5x-FAD*) (**Figure 16B-C**) or biological sex (**Figure 16D-E**). No statistically significant differences were observed in relative collagen IV volume in the male ( $6.24 \pm 1.79$  vs  $5.73 \pm 0.66$ , wild-type vs. *5x-FAD*,  $p = 0.769$ ) and female groups ( $5.35 \pm 1.67$  vs  $6.68 \pm 0.70$ , wild-type vs. *5x-FAD*,  $p = 0.409$ ). When comparing males and females of the same genotype, no statistically significant differences were observed among the wild-type ( $6.24 \pm 1.79$  vs  $5.35 \pm 1.67$ , males vs. females,  $p = 0.739$ ) and *5x-FAD* ( $5.73 \pm 0.66$  vs  $6.68 \pm 0.70$ , males vs. females,  $p = 0.342$ ) groups. Similarly, capillary counts (**Figure 17A**) showed that there were no significant differences between male wild-type and *5x-FAD* mice ( $31.30 \pm 0.86$  vs  $29.33 \pm 1.34$ , wild-type vs. *5x-FAD*,  $p = 0.28$ ) (**Figure 17B**) or female wild-type and *5x-FAD* mice ( $31.53 \pm 1.34$  vs  $29.83 \pm 2.56$ , wild-type vs. *5x-FAD*,  $p = 0.649$ ) (**Figure 17C**). Also, no sex differences were observed between the biological sexes among the wild-type ( $31.30 \pm 0.86$  vs  $31.53 \pm 1.34$ , males vs. females,  $p = 0.885$ ) (**Figure 17D**) and *5x-FAD* ( $29.33 \pm 1.34$  vs  $29.83 \pm 2.56$ , males vs. females,  $p = 0.8593$ ) (**Figure 17E**) mice. Thus, we conclude that microvascular rarefaction does not occur in *5x-FAD* mice at the age studied.





**Figure 16.** Relative collagen IV volume is unchanged between 3-month-old wild-Type and 5x-FAD male and female mice. Representative images taken from each Z-stack are shown for these mice showing collagen IV labeling in red (A). The data are represented as volume of the Z-stack occupied by collagen IV compared between the wild-type and 5x-FAD groups of males (B) and female (C) mice. Male and female sexes were also compared between the wild-type (D) and 5x-FAD (E) groups. Data are expressed as means  $\pm$  SEM. Two-tailed *Student's T*-test.



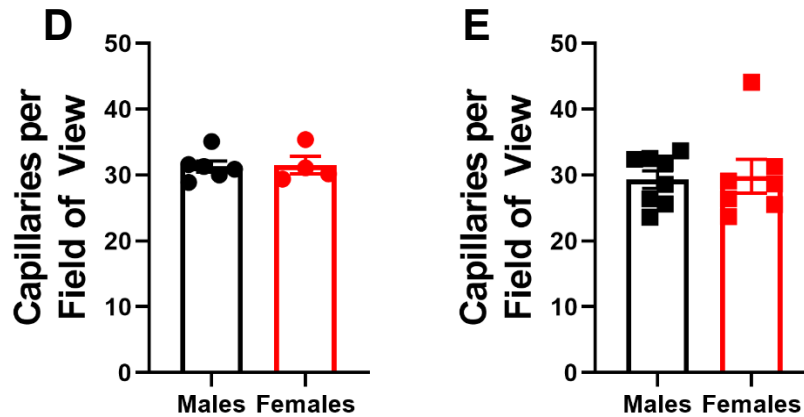


**Figure 17.** Number of capillaries is unchanged between 3-month-old Wild-Type and 5x-FAD male and female mice. Representative max intensity projections from collagen IV Z-stacks for these mice are shown for these mice with collagen IV labeling in red (A). The data are represented as capillaries per field of view compared between the wild-type and 5x-FAD groups for male (B) and female (C) mice. Male and female sexes were also compared between the wild-type (D) and 5x-FAD (E) groups. Data are expressed as means  $\pm$  SEM. \*  $p < 0.05$ , two-tailed *Student's* T-test.

### ***Perivascular A $\beta$ accumulation in pial blood vessels, but not in the parenchymal microcirculation of 5x-FAD***

CAA was then measured in these mice as percent of the collagen IV signal that is also occupied by A $\beta$  for the parenchymal vessels and the number of CAA positive vessels for the pial vessel data. Male and female wild-type mice did not exhibit A $\beta$ -pE3- or A $\beta$ -positive plaques, therefore they did not display CAA in parenchymal or pial vessels (Figure 18 and Figure 20). However, CAA was observed in both males and female 5x-FAD (Figure 19 and Figure 21), with regional differences. Little perivascular A $\beta$  accumulation was observed in the parenchymal microcirculation, without sex differences, suggesting that 5x-FAD are not an appropriate model of parenchymal CAA ( $1.95 \pm 0.30$  vs  $2.31 \pm 0.71$ , males vs females,  $p = 0.633$ ) (Figure 19B). On the other hand, perivascular A $\beta$  plaques were evident in the pial vessels, and our analysis showed that approximately 50% of surface vessels show mural A $\beta$  accumulation, without

significant differences between male and female *5x-FAD* ( $46.95 \pm 10.73$  vs  $41.44 \pm 8.18$ , males vs. females,  $p = 0.689$ ) (Figure 21B).

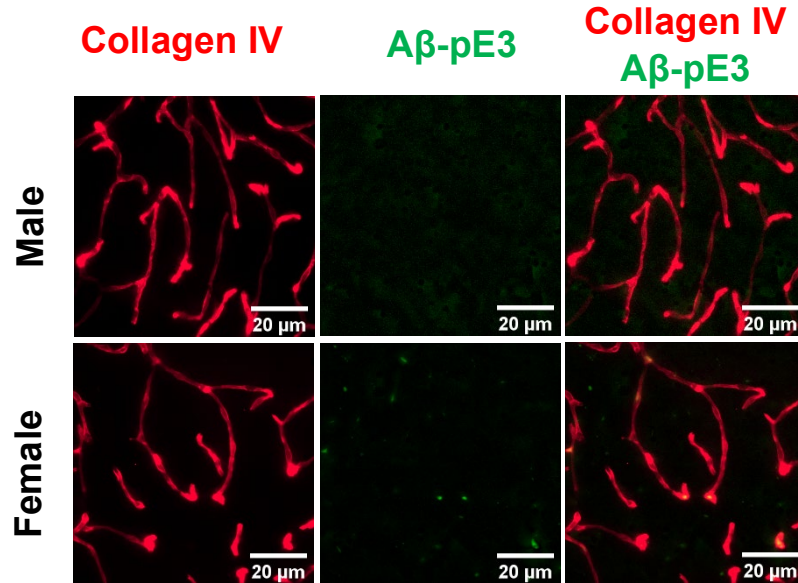


**Figure 18.** No accumulation of *Aβ-pE3* is observed on parenchymal microvasculature of 3-month-old wild-type mice. Representative max intensity projections of Z-stacks of collagen IV shown in red and *Aβ-pE3* shown in green for male and female wild-type mice.

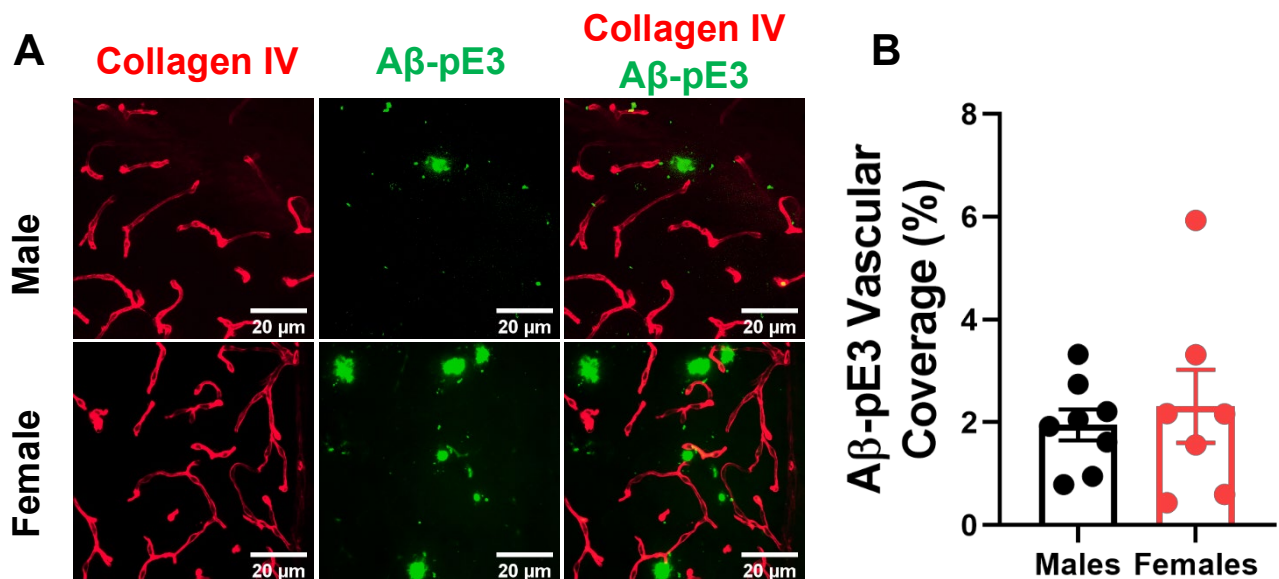


**Figure 19.** *Low accumulation of A $\beta$ -pE3 on the parenchymal microvasculature of 3-month-old 5x-FAD mice without sex differences.* Representative max intensity projections of Z-stacks are shown with collagen IV in red and A $\beta$ -pE3 in green for 5x-FAD male and female mice (A). The data are represented as collagen IV volume that is occupied by A $\beta$ -pE3 expressed as a percentage for the male and female 5x-FAD mice (B). No statistically significant differences were observed in the A $\beta$ -pE3 vascular coverage between males versus females ( $1.95 \pm 0.30$  vs  $2.31 \pm 0.71$ ,  $p = 0.633$ ). Data are expressed as means  $\pm$  SEM. Two-tailed Student's T-test.

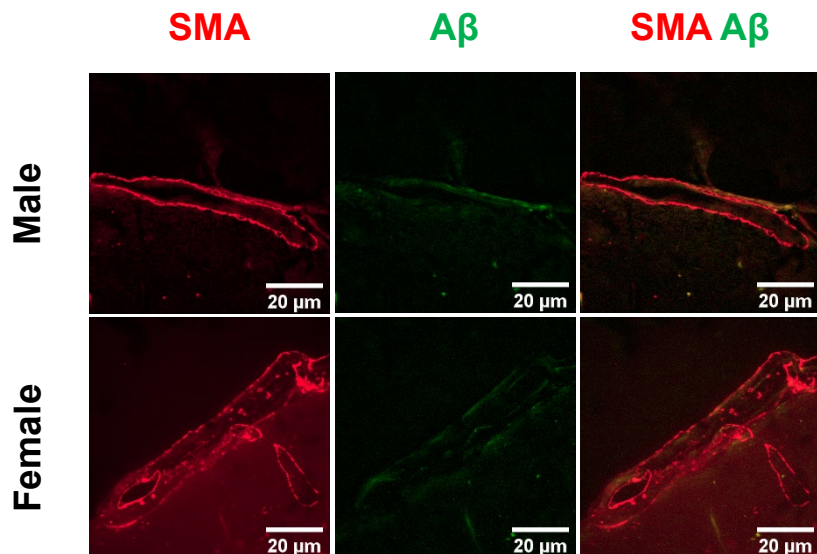


**Figure 20.** *No perivascular A $\beta$  accumulation in the pial circulation of 3-month-old wild-type mice.* Representative images of alpha-smooth muscle actin in red and A $\beta$  in green for male and female wild-type mice.

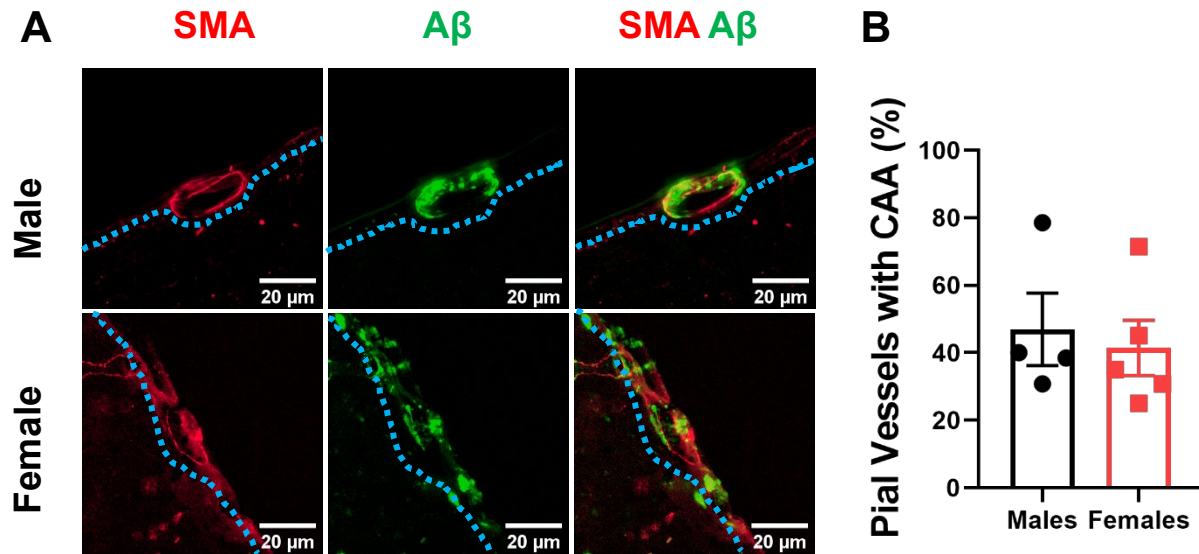


**Figure 21.** Perivascular  $A\beta$  accumulation in the pial circulation is not dependent on biological sex. Representative images of  $\alpha$ -smooth muscle actin in red and  $A\beta$  in green for  $5x$ -FAD male and female mice (A). The data are represented as percent of pial vessels that exhibit CAA for the male and female  $5x$ -FAD mice (B). No statistically significant differences were observed in the percent of pial vessels exhibiting CAA between the males versus females ( $46.95 \pm 10.73$  vs  $41.44 \pm 8.18$ ,  $p = 0.689$ ). Data are expressed as means  $\pm$  SEM. Two-tailed *Student's* T-test.

## Discussion

In this study, we observed that 3-month-old  $5x$ -FAD mice exhibit  $A\beta$  and  $A\beta$ -pE3 plaques throughout the brain with particular focus on the cortex and hippocampus.  $A\beta$  and  $A\beta$ -pE3 plaques were not observed in the cortex and hippocampus of 1-month-old  $5x$ -FAD mice but were observed in these mice at 2 months of age suggesting that plaque accumulation begins between 1 and 2 months post-birth. No sex differences were observed in overall  $A\beta$  plaques in cortex and hippocampus the three age groups studied. However, at 3 months of age, female  $5x$ -FAD mice displayed significantly higher  $A\beta$ -pE3 plaque density and coverage compared to males in both regions. This sex difference was not observed at 1- or 2-months

of age. Additionally, 3-month-old *5x-FAD* female mice were observed to have a greater percentage of A $\beta$  plaques that contain A $\beta$ -pE3 at their core despite there being no sex difference in the density of A $\beta$ -pE3-positive A $\beta$  plaques. We also noted that A $\beta$ -pE3 also labeled plaques that were negative for A $\beta$ , but observed no sex differences in the density of percent of these plaques. We observed little to no accumulation of A $\beta$ -pE3 on the parenchymal vessels. Thus, we would predict that there is little to no accumulation of overall A $\beta$  on the parenchymal vessel as well. However, we did observe accumulation of A $\beta$  on roughly 50% of  $\alpha$ -smooth muscle actin-positive pial vessels of these mice, without sex differences. As expected, wild-type mice of either gender did not display CAA on parenchymal nor pial vessels. In line with our observation that CAA was seldom observed on parenchymal vessels, we observed that collagen IV volume and capillary numbers were similar between the wild-types and *5x-FAD* mice of both sexes. Thus, 3-month-old *5x-FAD* mice may display A $\beta$  plaques, but do not exhibit capillary or microvascular rarefaction in the brain. Also, sex differences may be present in A $\beta$ -pE3 accumulation.

The results of the present study suggest that A $\beta$ -pE3, but not overall A $\beta$  plaque pathology, may be exacerbated in female *5x-FAD* mice in the cerebral cortex and hippocampus compared to male mice at 3-months of age. However, several studies noted that female *5x-FAD* mice possessed a greater A $\beta$  plaque load<sup>103,104</sup> and protein level<sup>97,105</sup> compared to age-matched male mice. Our results suggest that there may be a trend toward a greater A $\beta$  plaque density in the cortex of female *5x-FAD* mice, but otherwise no differences were observed in A $\beta$  cortical plaque area, hippocampal plaque density, or hippocampal plaque area. Although studies have shown that A $\beta$ -pE3 is produced in the brains of *5x-FAD* mice<sup>106,107</sup>, plaques consisting of this isoform have not been compared between male and female *5x-FAD* mice. The observations from this part of the study suggest that the elevated A $\beta$ -pE3 in the female mice compared to the male mice would favor greater overall A $\beta$  plaque accumulation due to the elevated levels of this seeding species. This is further supported by our observation that female *5x-FAD* mice had a greater proportion of overall A $\beta$  plaques that are positive for A $\beta$ -pE3 compared to *5x-FAD* male mice. The association between A $\beta$ -pE3 and A $\beta$  plaque was observed in another study, where overexpression of QC, the enzyme responsible

for generating A $\beta$ -pE3, in *5x-FAD* mice resulted in increased A $\beta$ -pE3 and overall A $\beta$  plaques in the cerebral cortex<sup>108</sup>. However, the elevated A $\beta$ -pE3 plaques in the females could be attributed to greater A $\beta$  production, resulting in more substrate as A $\beta$ -pE3 is derived from A $\beta$ . Another possibility is that QC could also be differentially modulated by the sex of these mice. As mentioned previously, one human study suggested that glutamyl cyclase activity may be higher in women<sup>55</sup>. Additionally, QC mRNA levels may possibly be regulated by the sex hormone, estrogen, as suggested in studies looking at non-neuronal cell types such as endometrium<sup>109</sup> and bronchial epithelial cells<sup>110</sup>. If these observations also do apply to neurons, then the differential modulation of QC could account for these observations.

One factor that has been hypothesized to play a major role in sex differences in AD is the hormone estrogen. Several human studies suggest that loss of estrogen during menopause may play a role in the increased likelihood of a women to develop AD<sup>111,112</sup>. One study looking more specifically at 3-4 – month-old female *5x-FAD* mice, observed that serum estrogen levels were not significantly different compared with age- and sex-matched wild-types<sup>113</sup>. However, a different study noted that 3-month-old female *5x-FAD* mice had relatively lower hippocampal mRNA levels of aromatase, a key enzyme in the synthesis of estrogen, compared to age- and sex-matched wild types<sup>114</sup>. Although systemic estrogen levels in female *5x-FAD* mice do not appear to differ compared to female wild-types, production of estrogen may be impaired locally in specific brain regions at 3 months of age. Additionally, the *Thy1* promoter used to drive expression of mutant APP in these mice contains an estrogen response element (ERE) upstream of the *5x-FAD* transgene in the *Thy1* regulatory region<sup>105</sup>. The presence of an ERE in the *Thy1* promoter suggests that endogenous estrogen in female mice could drive increased production of A $\beta$ <sup>105</sup>. Elevated A $\beta$  levels in females compared to males have also been observed in other mouse models of AD that use the *Thy1* promoter such as the *3xTgAD*<sup>115,116</sup> and *APP/PS1*<sup>117,118</sup> mice<sup>95</sup>. The sex differences in A $\beta$ -pE3 could be partly due to this ERE on the *Thy1* promoter generating greater quantities of A $\beta$  that could be processed by QC. If this observation is simply an artifact of the gene construct, then removal or inhibition of estrogen would potentially decrease plaque load. However, experiments where estrogen levels are altered through

ovariectomy or aromatase inhibition other *Thy1*-dependent AD mouse models observed that such treatments, which were done at an age prior to the onset of A $\beta$  plaques in those models, appeared to elevate A $\beta$  levels<sup>119,120</sup>. Taken together, whether the presence of the ERE in the *Thy1* promoter plays a role in the elevated A $\beta$  pathology in the female *5x-FAD* mice compared to males is not entirely clear given the observations that hippocampal<sup>114</sup>, but not systemic<sup>113</sup>, estrogen production may be impaired or possibly lower in females compared to males. It is possible that the ERE in the *Thy1* promoter plays a negligible or minor role in enhancing A $\beta$  accumulation in female mice. Thus, any sex differences in A $\beta$  pathology in the *5x-FAD* model are not solely an artifact of the AD transgenes. This is further supported by studies where removal of estrogen in other *Thy1* mouse models of AD was not been observed to directly decrease the plaque load<sup>119,120</sup>. For example, it has been observed that subjecting *5x-FAD* mice to stress preferentially elevated hippocampal plaque load in females compared to males via an upregulation of  $\beta$ -secretase, BACE1 and APP<sup>121</sup>. Interestingly, the study noted that *5x-FAD* females not subjected to behavioral stress had a hippocampal plaque load and A $\beta_{1-42}$  levels comparable to *5x-FAD* males<sup>121</sup>. Although estrogen may influence the presence or lack of sex differences in this mouse model, it may not be the sole factor.

Tracking the A $\beta$  plaque density in 1- and 2-month-old *5x-FAD* mice revealed no sex differences in accumulation in the cortex and hippocampus. In accordance with another study<sup>97</sup>, we observed that the accumulation of A $\beta$  in *5x-FAD* begins between 1 - 2 months of age. Interestingly, we observed that between 2 and 3 months of age, the plaque density in the male and female mice seemed to increase dramatically. The *Thy1* promoter, the promoter that drives A $\beta$  expression in this mouse model, has been suggested to turn on around postnatal day 7<sup>122, 123</sup> and has been suggested to be developmentally regulated<sup>124</sup>. Beyond postnatal day 14, protein expression driven by *Thy1* has been suggested to increase dramatically and continue to increase into adulthood<sup>123,124</sup>. However, A $\beta$  production has not been observed in the *5x-FAD* mouse model until around 1.5 months of age<sup>97</sup>. Thus, it is possible that prior to 1-2 months of age, A $\beta$  production exists at low levels that are not able to be detected using current protein quantification methods. Another possibility is that the levels of A $\beta$  do not exceed the capacity of different clearance mechanisms in

the mouse brain<sup>125</sup>. Thus, the occurrence of A $\beta$  plaques around 1-2 months of age could possibly reflect the inability of the brain's clearance systems to handle elevated levels of A $\beta$  that resulted from increased *Thy1* activity. Whether these factors influence the onset and/or rapid accumulation of A $\beta$  accumulation needs further exploration. It has been suggested that the plaque density of these mice may continue to increase beyond 3 months of age and eventually plateau for males at 10 months of age, but not females<sup>103</sup>. Our preliminary data suggests that 1-year-old *5x-FAD* males do display more plaques compared to 3-month-old males (not shown), however we did not measure the plaque density for mice between those two ages nor did we measure plaque density for older *5x-FAD* females. Thus, for mice of either sex, we are unable to determine if the plaque density plateaus within that age range or experiences an even more dramatic increase compared to what we observed at 2 - 3 months of age. The sudden, dramatic increase in A $\beta$  plaque density between 2 and 3 months of age observed in this study could reflect the kinetics of A $\beta$  aggregation, whereby A $\beta$  aggregation undergoes an exponential phase<sup>126</sup>, and this sudden increase in plaques has also been observed in the *5x-FAD* mouse model<sup>103,97</sup> as well as other mouse models of AD, albeit at different ages<sup>127-129</sup>. Based on the study conducted by Bhattacharya *et al.*, plaque density seems to increase most dramatically between 8-10 months for male *5x-FAD* mice and 3-4 months for female mice<sup>103</sup>. This time course of accumulation is likely due to multiple factors such as the transgene promoter, the mutations within the transgene itself, location of the transgene on the chromosome, and the genetic background on which it is expressed<sup>95</sup>.

For the most part, the plaque counts using thioflavin-T corresponded with counts using the A $\beta$ -mOC64 antibody. However, there were subtle differences in plaque detection likely reflecting differences in the methods used to label the A $\beta$  plaques. Thioflavin-T is a benzothiazole dye that binds to structures rich in beta sheets such as A $\beta$ <sup>98</sup>. When thioflavin-T binds to amyloid fibrils, thioflavin-T fluoresces brightly with an excitation and emission maxima of 450 and 485nm, respectively<sup>130</sup>. Although thioflavin-T is often used for identification and analysis of amyloid fibrils, it has also been shown to bind to non-A $\beta$  structures such as hydrophobic pockets in globular proteins such as albumin<sup>131</sup> and acetylcholinesterase<sup>132</sup>.

Meanwhile, the A $\beta$ -mOC64 antibody has been demonstrated to label primarily A $\beta$ <sub>1-42</sub> and, in some instances, A $\beta$ <sub>1-40</sub><sup>133</sup>. We noted that thioflavin-T appeared to label less plaques than the A $\beta$ -mOC64 antibody suggesting that the thioflavin-T stain is not as sensitive. The lower sensitivity of chemical staining methods, such as thioflavin-T, compared to antibody detection has also been noted in a different study comparing thioflavin S, another fluorescent dye similar to thioflavin-T used to detect A $\beta$  plaques, and a different A $\beta$  antibody, 4G8<sup>134</sup>. This is more apparent when we were staining the 2-month-old *5x-FAD* female brains. We also noted that thioflavin-T tended to yield a higher background than the A $\beta$ -mOC64 antibody due to its ability to bind to other structures as mentioned previously. Thus, thioflavin-T is appropriate for labeling brains that already display plaques but may be less useful in labeling plaques in their earlier stages, likely due to the lower beta sheet content of these earlier plaques.

Although 3-month-old *5x-FAD* mice exhibit A $\beta$  plaque pathology throughout the brain parenchyma, there was little to no A $\beta$  accumulation around the parenchymal vessels as cerebral amyloid angiopathy, and there were no sex differences in the quantities that were present. Another study looking more specifically at the microvessels also noted little to no parenchymal CAA in these mice<sup>135</sup>. However, A $\beta$  accumulation was observed on the pial vessels<sup>136</sup> and, in some instances, on large cortical vessels<sup>137</sup>. Additionally, the *5x-FAD* mice studied here did not display blood vessel or capillary rarefaction in the parenchyma when compared to their age- and sex-matched wild-types, suggesting this mouse model does not exhibit vascular or microvascular alterations at the histological level, which is further supported by the lack of parenchymal CAA. We observed that the relative volume of collagen IV throughout the brain appears to be unchanged. However, it should be noted that several studies did observe reductions in blood vessels in specific regions of the brain in *5x-FAD* mice as young as 2-5 months of age, not stratified by gender<sup>136,138</sup>. Giannoni *et al.* observed decreases in vessel length in *5x-FAD* mice starting at 2 months of age in the parietal cortices using FITC-albumin perfused brain slices<sup>136</sup>. Meanwhile, Ahn *et al.* observed decreased immunoreactivity of GLUT-1, a possible marker for the brain vasculature, in *5x-FAD* brain slices of 4.5-month-old mice<sup>138</sup>. Although our results suggest no reduction in capillary number or overall collagen

IV volume in the 3-month-old *5x-FAD* brain, it is possible that there are regional variations in capillary rarefaction, but due to our method of quantification, we are not able to resolve those spatial differences. Alternatively, the lack of parenchymal CAA and capillary rarefaction could be due to the preferential production of A $\beta$ <sub>1-42</sub> over A $\beta$ <sub>1-40</sub> in *5x-FAD* mice. *5x-FAD* mice have been shown to produce greater amounts of A $\beta$ <sub>1-42</sub> relative to A $\beta$ <sub>1-40</sub><sup>97</sup>. As discussed previously, A $\beta$ <sub>1-40</sub> is the predominant form that comprises perivascular plaques in CAA<sup>26</sup>. Thus, these mice would not be expected to develop CAA or display microvascular alterations. However, *5x-FAD* mice still produce A $\beta$ <sub>1-40</sub> at elevated levels<sup>97</sup>, even exceeding those of age-matched *Tg-SwDI* mice, a mouse model of microvessel CAA<sup>139</sup>. Interestingly, in ELISAs of whole brain homogenates, Oakley *et al.* observed that A $\beta$ <sub>1-40</sub> accumulation continues to increase with age for *5x-FAD* mice of either gender, and plateaus in males, but not in females, around 6 months of age<sup>97</sup>.

Whether these histological findings correlate with motor or behavioral outcomes in these mice has not been explored or addressed in this current study but has been explored to a limited extent in studies conducted by other groups. At around 3-4 months of age, observations from several studies suggest that motor function is not impaired in male or female *5x-FAD* mice<sup>140,141</sup>. However, decline in motor functions were observed at later ages with potential sex differences<sup>140,141</sup>. Due to the inconsistency of the results across different ages for the two genders with some ages ranges displaying worse motor function in males, females, or neither, whether sex differences exist remains unclear<sup>140</sup>. We have preliminary data that female *5x-FAD* mice 3-4 months of age may display cognitive impairment, but we do not have data on whether males at this age are cognitively impaired (not shown). Whether these mice possess memory deficits at 1, 2, or 3 months of age is not entirely clear with some studies observing impaired spatial memory<sup>142,143</sup> and others reporting non-impaired<sup>97,144</sup> spatial memory. However, several studies do suggest that motor<sup>140,141</sup> and behavioral deficits<sup>97,144</sup> may appear in older *5x-FAD*. Thus, onset of motor and memory impairments may not directly correlate with the early onset of A $\beta$  deposition, but rather may manifest later in *5x-FAD* mice.

This suggests that A $\beta$  accumulation precedes synaptic loss or neuronal cell death in this model, which has been observed to occur at around 4-6 months of age<sup>97</sup>.

In conclusion, the observations from this current study suggest that A $\beta$ -pE3 levels are elevated in 3-month-old female *5x-FAD* mice compared to age matched males, however, no statistically significant differences were observed in overall A $\beta$  levels. At this age, there does not appear to be microvascular alterations from a histological standpoint. This is correlated with relatively little to CAA in the brain parenchyma. However, CAA was observed on approximately 50% of the pial vessels. Thus, at the age studied, despite the elevated A $\beta$ -pE3 plaque load of the female *5x-FAD* mice, the microvasculature appears relatively unaffected. Additionally, plaque accumulation appears to start between 1 and 2 months with no statistically significant sex differences observed. However, provided the limited sample size of some of these studies and the fact that the gene construct of this mouse model may possess an ERE, caution must be taken when interpreting these observations. Given these observations, future studies will be aimed toward elucidating the mechanisms that account for these sex differences, or lack thereof, in these mice as well as further exploring whether this plaque load alters the physiological function of the cerebral vasculature. Thus, these data can help set the groundwork for further studies that set out to identify pharmacologic targets that may be useful in the effective treatment of AD for both the male and female sexes.

## References

1. Hebert LE, Weuve J, Scherr PA, Evans DA. Alzheimer disease in the United States (2010-2050) estimated using the 2010 census. *Neurology*. 2013;80(19):1778-1783. doi:10.1212/WNL.0b013e31828726f5
2. Alzheimer's Association. 2020 Alzheimer's disease facts and figures. *Alzheimers Dement* 2020;16:391–460.
3. GBD 2016 Dementia Collaborators. Global, regional, and national burden of Alzheimer's disease and other dementias, 1990-2016: a systematic analysis for the Global Burden of Disease Study 2016. *Lancet Neurol*. 2019;18(1):88-106. doi:10.1016/S1474-4422(18)30403-4
4. Beam CR, Kaneshiro C, Jang JY, Reynolds CA, Pedersen NL, Gatz M. Differences Between Women and Men in Incidence Rates of Dementia and Alzheimer's Disease. *J Alzheimers Dis*. 2018;64(4):1077-1083. doi:10.3233/JAD-180141
5. Viña J, Lloret A. Why women have more Alzheimer's disease than men: gender and mitochondrial toxicity of amyloid-beta peptide. *J Alzheimers Dis*. 2010;20 Suppl 2:S527-33. doi: 10.3233/JAD-2010-100501. PMID: 20442496.
6. Letenneur L, Gilleron V, Commenges D, Helmer C, Orgogozo JM, Dartigues JF. Are sex and educational level independent predictors of dementia and Alzheimer's disease? Incidence data from the PAQUID project. *J Neurol Neurosurg Psychiatry*. 1999;66(2):177-183. doi:10.1136/jnnp.66.2.177
7. Fratiglioni L, Launer LJ, Andersen K, Breteler MM, Copeland JR, Dartigues JF, Lobo A, Martinez-Lage J, Soininen H, Hofman A. Incidence of dementia and major subtypes in Europe: A collaborative study of population-based cohorts. Neurologic Diseases in the Elderly Research Group. *Neurology*. 2000;54(11 Suppl 5):S10-S15.
8. van der Flier WM, Scheltens P. Epidemiology and risk factors of dementia. *J Neurol Neurosurg Psychiatry*. 2005;76 Suppl 5(Suppl 5):v2-v7. doi:10.1136/jnnp.2005.082867
9. Edland SD, Rocca WA, Petersen RC, Cha RH, Kokmen E. Dementia and Alzheimer disease incidence rates do not vary by sex in Rochester, Minn. *Arch Neurol*. 2002;59(10):1589-1593. doi:10.1001/archneur.59.10.1589
10. Kawas C, Gray S, Brookmeyer R, Fozard J, Zonderman A. Age-specific incidence rates of Alzheimer's disease: the Baltimore Longitudinal Study of Aging. *Neurology*. 2000;54(11):2072-2077. doi:10.1212/wnl.54.11.2072
11. Matthews FE, Arthur A, Barnes LE, Bond J, Jagger C, Robinson L, Brayne C; Medical Research Council Cognitive Function and Ageing Collaboration. A two-decade comparison of prevalence of dementia in individuals aged 65 years and older from three geographical areas of England: results of the Cognitive Function and Ageing Study I and II. *Lancet*. 2013;382(9902):1405-1412. doi:10.1016/S0140-6736(13)61570-6
12. Murphy MP, LeVine H 3rd. Alzheimer's disease and the amyloid-beta peptide. *J Alzheimers Dis*. 2010;19(1):311-323. doi:10.3233/JAD-2010-1221
13. Atri A. The Alzheimer's Disease Clinical Spectrum: Diagnosis and Management. *Med Clin North Am*. 2019;103(2):263-293. doi:10.1016/j.mcna.2018.10.009

14. Pini L, Pievani M, Bocchetta M, Altomare D, Bosco P, Cavedo E, Galluzzi S, Marizzoni M, Frisoni GB. Brain atrophy in Alzheimer's Disease and aging. *Ageing Res Rev.* 2016;30:25-48. doi:10.1016/j.arr.2016.01.002
15. Tensil M, Hessler JB, Gutsmiel M, Riedl L, Grimmer T, Diehl-Schmid J. Sex Differences in Neuropsychological Test Performance in Alzheimer's Disease and the Influence of the ApoE Genotype. *Alzheimer Dis Assoc Disord.* 2018;32(2):145-149. doi:10.1097/WAD.0000000000000229
16. Chapman RM, Mapstone M, Gardner MN, Sandoval TC, McCrary JW, Guillily MD, Reilly LA, DeGrush E. Women have farther to fall: gender differences between normal elderly and Alzheimer's disease in verbal memory engender better detection of Alzheimer's disease in women. *J Int Neuropsychol Soc.* 2011;17(4):654-662. doi:10.1017/S1355617711000452
17. Hua X, Hibar DP, Lee S, et al. Sex and age differences in atrophic rates: an ADNI study with n=1368 MRI scans. *Neurobiol Aging.* 2010;31(8):1463-1480. doi:10.1016/j.neurobiolaging.2010.04.033
18. Ardekani BA, Convit A, Bachman AH. Analysis of the MIRIAD Data Shows Sex Differences in Hippocampal Atrophy Progression. *J Alzheimers Dis.* 2016;50(3):847-857. doi:10.3233/JAD-150780
19. Filon, J. R., Intorcchia, A. J., Sue, L. I., Vazquez Arreola, E., Wilson, J., Davis, K. J., Sabbagh, M. N., Belden, C. M., Caselli, R. J., Adler, C. H., Woodruff, B. K., Rapsack, S. Z., Ahern, G. L., Burke, A. D., Jacobson, S., Shill, H. A., Driver-Dunckley, E., Chen, K., Reiman, E. M., Beach, T. G., ... Serrano, G. E. Gender Differences in Alzheimer Disease: Brain Atrophy, Histopathology Burden, and Cognition. *J Neuropathol Exp Neurol.* 2016;75(8):748-754. doi:10.1093/jnen/nlw047
20. Ferretti, M. T., Iulita, M. F., Cavedo, E., Chiesa, P. A., Schumacher Dimech, A., Santuccion Chadha, A., Baracchi, F., Girouard, H., Misoch, S., Giacobini, E., Depypere, H., Hampel, H., & Women's Brain Project and the Alzheimer Precision Medicine Initiative. Sex differences in Alzheimer disease - the gateway to precision medicine. *Nat Rev Neurol.* 2018;14(8):457-469. doi:10.1038/s41582-018-0032-9
21. Hardy JA, Higgins GA. Alzheimer's disease: the amyloid cascade hypothesis. *Science.* 1992;256(5054):184-185. doi:10.1126/science.1566067
22. Selkoe DJ. Alzheimer's disease: genes, proteins, and therapy. *Physiol Rev.* 2001;81(2):741-766. doi:10.1152/physrev.2001.81.2.741
23. Arai H, Lee VM, Messinger ML, Greenberg BD, Lowery DE, Trojanowski JQ. Expression patterns of beta-amyloid precursor protein (beta-APP) in neural and nonneural human tissues from Alzheimer's disease and control subjects. *Ann Neurol.* 1991;30(5):686-693. doi:10.1002/ana.410300509
24. Golde TE, Estus S, Usiak M, Younkin LH, Younkin SG. Expression of beta amyloid protein precursor mRNAs: recognition of a novel alternatively spliced form and quantitation in Alzheimer's disease using PCR. *Neuron.* 1990;4(2):253-267. doi:10.1016/0896-6273(90)90100-t
25. Forloni G, Demicheli F, Giorgi S, Bendotti C, Angeretti N. Expression of amyloid precursor protein mRNAs in endothelial, neuronal and glial cells: modulation by interleukin-1. *Brain Res Mol Brain Res.* 1992;16(1-2):128-134. doi:10.1016/0169-328x(92)90202-m
26. Haass C, Kaether C, Thinakaran G, Sisodia S. Trafficking and proteolytic processing of APP. *Cold Spring Harb Perspect Med.* 2012;2(5):a006270. doi:10.1101/cshperspect.a006270 Suzuki N, Iwatsubo T, Odaka A, Ishibashi Y, Kitada C, Ihara Y. High tissue content of soluble beta 1-40 is linked to cerebral amyloid angiopathy. *Am J Pathol.* 1994;145(2):452-460.

27. Scheuner D, Eckman C, Jensen M, Song X, Citron M, Suzuki N, Bird TD, Hardy J, Hutton M, Kukull W, Larson E, Levy-Lahad E, Viitanen M, Peskind E, Poorkaj P, Schellenberg G, Tanzi R, Wasco W, Lannfelt L, Selkoe D, Younkin S. Secreted amyloid beta-protein similar to that in the senile plaques of Alzheimer's disease is increased in vivo by the presenilin 1 and 2 and APP mutations linked to familial Alzheimer's disease. *Nat Med.* 1996;2(8):864-870. doi:10.1038/nm0896-864
28. Bekris LM, Yu CE, Bird TD, Tsuang DW. Genetics of Alzheimer disease. *J Geriatr Psychiatry Neurol.* 2010;23(4):213-227. doi:10.1177/0891988710383571
29. Jarrett JT, Berger EP, Lansbury PT Jr. The carboxy terminus of the beta amyloid protein is critical for the seeding of amyloid formation: implications for the pathogenesis of Alzheimer's disease. *Biochemistry.* 1993;32(18):4693-4697. doi:10.1021/bi00069a001
30. Roher, A. E., Lowenson, J. D., Clarke, S., Woods, A. S., Cotter, R. J., Gowing, E., & Ball, M. J. beta-Amyloid-(1-42) is a major component of cerebrovascular amyloid deposits: implications for the pathology of Alzheimer disease. *Proc Natl Acad Sci U S A.* 1993;90(22):10836-10840. doi:10.1073/pnas.90.22.10836
31. Scheuner D, Eckman C, Jensen M, Song X, Citron M, Suzuki N, Bird TD, Hardy J, Hutton M, Kukull W, Larson E, Levy-Lahad E, Viitanen M, Peskind E, Poorkaj P, Schellenberg G, Tanzi R, Wasco W, Lannfelt L, Selkoe D, Younkin S. Secreted amyloid beta-protein similar to that in the senile plaques of Alzheimer's disease is increased in vivo by the presenilin 1 and 2 and APP mutations linked to familial Alzheimer's disease. *Nat Med.* 1996;2(8):864-870. doi:10.1038/nm0896-864
32. De Jonghe C, Esselens C, Kumar-Singh S, Craessaerts K, Serneels S, Checler F, Annaert W, Van Broeckhoven C, De Strooper B. Pathogenic APP mutations near the gamma-secretase cleavage site differentially affect Abeta secretion and APP C-terminal fragment stability. *Hum Mol Genet.* 2001;10(16):1665-1671. doi:10.1093/hmg/10.16.1665
33. Filon, J. R., Intorcica, A. J., Sue, L. I., Vazquez Arreola, E., Wilson, J., Davis, K. J., Sabbagh, M. N., Belden, C. M., Caselli, R. J., Adler, C. H., Woodruff, B. K., Rapsack, S. Z., Ahern, G. L., Burke, A. D., Jacobson, S., Shill, H. A., Driver-Dunckley, E., Chen, K., Reiman, E. M., Beach, T. G., ... Serrano, G. E. Gender Differences in Alzheimer Disease: Brain Atrophy, Histopathology Burden, and Cognition. *J Neuropathol Exp Neurol.* 2016;75(8):748-754. doi:10.1093/jnen/nlw047
34. Miller FD, Hicks SP, D'Amato CJ, Landis JR. A descriptive study of neuritic plaques and neurofibrillary tangles in an autopsy population. *Am J Epidemiol.* 1984;120(3):331-341. doi:10.1093/oxfordjournals.aje.a113897
35. Barnes LL, Wilson RS, Bienias JL, Schneider JA, Evans DA, Bennett DA. Sex differences in the clinical manifestations of Alzheimer disease pathology. *Arch Gen Psychiatry.* 2005;62(6):685-691. doi:10.1001/archpsyc.62.6.685
36. Shinohara M, Murray ME, Frank RD, Shinohara M, DeTure M, Yamazaki Y, Tachibana M, Atagi Y, Davis MD, Liu CC, Zhao N, Painter MM, Petersen RC, Fryer JD, Crook JE, Dickson DW, Bu G, Kanekiyo T. Impact of sex and APOE4 on cerebral amyloid angiopathy in Alzheimer's disease. *Acta Neuropathol.* 2016;132(2):225-234. doi:10.1007/s00401-016-1580-y36
37. Masters CL, Simms G, Weinman NA, Multhaup G, McDonald BL, Beyreuther K. Amyloid plaque core protein in Alzheimer disease and Down syndrome. *Proc Natl Acad Sci U S A.* 1985;82(12):4245-4249. doi:10.1073/pnas.82.12.4245

38. Selkoe DJ, Abraham CR, Podlisny MB, Duffy LK. Isolation of low-molecular-weight proteins from amyloid plaque fibers in Alzheimer's disease. *J Neurochem*. 1986;46(6):1820-1834. doi:10.1111/j.1471-4159.1986.tb08501.x
39. Jawhar S, Wirths O, Bayer TA. Pyroglutamate amyloid- $\beta$  (A $\beta$ ): a hatchet man in Alzheimer disease. *J Biol Chem*. 2011;286(45):38825-38832. doi:10.1074/jbc.R111.288308
40. Mori H, Takio K, Ogawara M, Selkoe DJ. Mass spectrometry of purified amyloid beta protein in Alzheimer's disease. *J Biol Chem*. 1992 Aug 25;267(24):17082-6. PMID: 1512246.
41. Cynis H, Scheel E, Saido TC, Schilling S, Demuth HU. Amyloidogenic processing of amyloid precursor protein: evidence of a pivotal role of glutaminyl cyclase in generation of pyroglutamate-modified amyloid-beta. *Biochemistry*. 2008;47(28):7405-7413.
42. Fischer WH, Spiess J. Identification of a mammalian glutaminyl cyclase converting glutaminyl into pyroglutamyl peptides. *Proc Natl Acad Sci U S A*. 1987;84(11):3628-3632. doi:10.1073/pnas.84.11.3628
43. Morawski M, Schilling S, Kreuzberger M, Waniek A, Jäger C, Koch B, Cynis H, Kehlen A, Arendt T, Hartlage-Rübsamen M, Demuth HU, Roßner S. Glutaminyl cyclase in human cortex: correlation with (pGlu)-amyloid- $\beta$  load and cognitive decline in Alzheimer's disease. *J Alzheimers Dis*. 2014;39(2):385-400. doi:10.3233/JAD-131535
44. Sevalle J, Amoyel A, Robert P, Fournié-Zaluski MC, Roques B, Checler F. Aminopeptidase A contributes to the N-terminal truncation of amyloid beta-peptide. *J Neurochem*. 2009;109(1):248-256. doi:10.1111/j.1471-4159.2009.05950.x
45. Schlenzig D, Cynis H, Hartlage-Rübsamen M, Zeitschel U, Menge K, Fothe A, Ramsbeck D, Spahn C, Wermann M, Roßner S, Buchholz M, Schilling S, Demuth HU. Dipeptidyl-Peptidase Activity of Meprin  $\beta$  Links N-truncation of A $\beta$  with Glutaminyl Cyclase-Catalyzed pGlu-A $\beta$  Formation. *J Alzheimers Dis*. 2018;66(1):359-375. doi:10.3233/JAD-171183
46. Antonyan A, Schlenzig D, Schilling S, Naumann M, Sharoyan S, Mardanyan S, Demuth HU. Concerted action of dipeptidyl peptidase IV and glutaminyl cyclase results in formation of pyroglutamate-modified amyloid peptides in vitro. *Neurochem Int*. 2018;113:112-119. doi:10.1016/j.neuint.2017.12.001
47. Perez-Garmendia R, Gevorkian G. Pyroglutamate-Modified Amyloid Beta Peptides: Emerging Targets for Alzheimer's Disease Immunotherapy. *Curr Neuropharmacol*. 2013;11(5):491-498. doi:10.2174/1570159X11311050004
48. He W, Barrow CJ. The A beta 3-pyroglutamyl and 11-pyroglutamyl peptides found in senile plaque have greater beta-sheet forming and aggregation propensities in vitro than full-length A beta. *Biochemistry*. 1999;38(33):10871-10877. doi:10.1021/bi990563r
49. Schilling, S., Lauber, T., Schaupp, M., Manhart, S., Scheel, E., Böhm, G., & Demuth, H. U. On the seeding and oligomerization of pGlu-amyloid peptides (in vitro). *Biochemistry*. 2006;45(41):12393-12399. doi:10.1021/bi0612667
50. Russo, C., Violani, E., Salis, S., Venezia, V., Dolcini, V., Damonte, G., Benatti, U., D'Arrigo, C., Patrone, E., Carlo, P., & Schettini, G. Pyroglutamate-modified amyloid beta-peptides--AbetaN3(pE)--strongly affect cultured neuron and astrocyte survival. *J Neurochem*. 2002;82(6):1480-1489. doi:10.1046/j.1471-4159.2002.01107.x

51. Iwatsubo T, Saido TC, Mann DM, Lee VM, Trojanowski JQ. Full-length amyloid-beta (1-42(43)) and amino-terminally modified and truncated amyloid-beta 42(43) deposit in diffuse plaques. *Am J Pathol*. 1996;149(6):1823-1830.
52. Moro ML, Phillips AS, Gaimster K, Paul C, Mudher A, Nicoll JAR, Boche D. Pyroglutamate and Isoaspartate modified Amyloid-Beta in ageing and Alzheimer's disease. *Acta Neuropathol Commun*. 2018;6(1):3. Published 2018 Jan 3. doi:10.1186/s40478-017-0505-x
53. Pivtoraiko VN, Abrahamson EE, Leurgans SE, DeKosky ST, Mufson EJ, Ikonovic MD. Cortical pyroglutamate amyloid- $\beta$  levels and cognitive decline in Alzheimer's disease. *Neurobiol Aging*. 2015;36(1):12-19. doi:10.1016/j.neurobiolaging.2014.06.021
54. De Kimpe L, van Haastert ES, Kaminari A, Zwart R, Rutjes H, Hoozemans JJ, Scheper W. Intracellular accumulation of aggregated pyroglutamate amyloid beta: convergence of aging and A $\beta$  pathology at the lysosome. *Age (Dordr)*. 2013;35(3):673-687. doi:10.1007/s11357-012-9403-0
55. Gunn AP, Wong BX, McLean C, Fowler C, Barnard PJ, Duce JA, Roberts BR; AIBL Research Group. Increased glutaminyl cyclase activity in brains of Alzheimer's disease individuals. *J Neurochem*. 2021;156(6):979-987. doi:10.1111/jnc.15114
56. Valenti MT, Bolognin S, Zanatta C, Donatelli L, Innamorati G, Pampanin M, Zanusso G, Zatta P, Dalle Carbonare L. Increased glutaminyl cyclase expression in peripheral blood of Alzheimer's disease patients. *J Alzheimers Dis*. 2013;34(1):263-271. doi:10.3233/JAD-120517
57. Csiszar, A., Tarantini, S., Fülöp, G. A., Kiss, T., Valcarcel-Ares, M. N., Galvan, V., Ungvari, Z., & Yabluchanskiy, A. Hypertension impairs neurovascular coupling and promotes microvascular injury: role in exacerbation of Alzheimer's disease. *Geroscience*. 2017;39(4):359-372. doi:10.1007/s11357-017-9991-9
58. Zlokovic BV. Neurovascular pathways to neurodegeneration in Alzheimer's disease and other disorders. *Nat Rev Neurosci*. 2011;12(12):723-738. Published 2011 Nov 3. doi:10.1038/nrn3114
59. Hecht M, Krämer LM, von Arnim CAF, Otto M, Thal DR. Capillary cerebral amyloid angiopathy in Alzheimer's disease: association with allocortical/hippocampal microinfarcts and cognitive decline. *Acta Neuropathol*. 2018;135(5):681-694. doi:10.1007/s00401-018-1834-y
60. Mandybur TI. Cerebral amyloid angiopathy: the vascular pathology and complications. *J Neuropathol Exp Neurol*. 1986;45(1):79-90.
61. Hunter JM, Kwan J, Malek-Ahmadi M, Maarouf CL, Kokjohn TA, Belden C, Sabbagh MN, Beach TG, Roher AE. Morphological and pathological evolution of the brain microcirculation in aging and Alzheimer's disease. *PLoS One*. 2012;7(5):e36893. doi:10.1371/journal.pone.0036893
62. Buée L, Hof PR, Bouras C, Delacourte A, Perl DP, Morrison JH, Fillit HM. Pathological alterations of the cerebral microvasculature in Alzheimer's disease and related dementing disorders. *Acta Neuropathol*. 1994;87(5):469-480. doi:10.1007/BF00294173
63. Kitaguchi H, Ihara M, Saiki H, Takahashi R, Tomimoto H. Capillary beds are decreased in Alzheimer's disease, but not in Binswanger's disease. *Neurosci Lett*. 2007;417(2):128-131. doi:10.1016/j.neulet.2007.02.021

64. Koizumi K, Wang G, Park L. Endothelial Dysfunction and Amyloid- $\beta$ -Induced Neurovascular Alterations. *Cell Mol Neurobiol*. 2016;36(2):155-165. doi:10.1007/s10571-015-0256-9
65. Bell MA, Ball MJ. Morphometric comparison of hippocampal microvasculature in ageing and demented people: diameters and densities. *Acta Neuropathol*. 1981;53(4):299-318. doi:10.1007/BF00690372
66. Damodarasamy M, Vernon RB, Pathan JL, Keene CD, Day AJ, Banks WA, Reed MJ. The microvascular extracellular matrix in brains with Alzheimer's disease neuropathologic change (ADNC) and cerebral amyloid angiopathy (CAA). *Fluids Barriers CNS*. 2020;17(1):60. Published 2020 Sep 29. doi:10.1186/s12987-020-00219-y
67. Richard E, van Gool WA, Hoozemans JJ, van Haastert ES, Eikelenboom P, Rozemuller AJ, van de Berg WD. Morphometric changes in the cortical microvascular network in Alzheimer's disease. *J Alzheimers Dis*. 2010;22(3):811-818. doi:10.3233/JAD-2010-100849
68. Hase Y, Ding R, Harrison G, Hawthorne E, King A, Gettings S, Platten C, Stevenson W, Craggs LJJ, Kalaria RN. White matter capillaries in vascular and neurodegenerative dementias. *Acta Neuropathol Commun*. 2019;7(1):16. Published 2019 Feb 7. doi:10.1186/s40478-019-0666-x
69. Fernandez-Klett F, Brandt L, Fernández-Zapata C, Abuelnor B, Middeldorp J, Sluijs JA, Curtis M, Faull R, Harris LW, Bahn S, Hol EM, Priller J. Denser brain capillary network with preserved pericytes in Alzheimer's disease. *Brain Pathol*. 2020;30(6):1071-1086. doi:10.1111/bpa.12897
70. Greenberg SM, Vernooij MW, Cordonnier C, Viswanathan A, Al-Shahi Salman R, Warach S, Launer LJ, Van Buchem MA, Breteler MM. Cerebral microbleeds: a guide to detection and interpretation. *Lancet Neurol*. 2009;8(2):165-174. doi:10.1016/S1474-4422(09)70013-4
71. Akoudad S, Wolters FJ, Viswanathan A, de Bruijn RF, van der Lugt A, Hofman A, Koudstaal PJ, Ikram MA, Vernooij MW. Association of Cerebral Microbleeds With Cognitive Decline and Dementia. *JAMA Neurol*. 2016;73(8):934-943. doi:10.1001/jamaneurol.2016.1017
72. Cordonnier C, van der Flier WM. Brain microbleeds and Alzheimer's disease: innocent observation or key player?. *Brain*. 2011;134(Pt 2):335-344. doi:10.1093/brain/awq321
73. Dierksen GA, Skehan ME, Khan MA, Jeng J, Nandigam RN, Becker JA, Kumar A, Neal KL, Betensky RA, Frosch MP, Rosand J, Johnson KA, Viswanathan A, Salat DH, Greenberg SM. Spatial relation between microbleeds and amyloid deposits in amyloid angiopathy. *Ann Neurol*. 2010;68(4):545-548. doi:10.1002/ana.22099
74. Oshima K, Akiyama H, Tsuchiya K, Kondo H, Haga C, Shimomura Y, Iseki E, Uchikado H, Kato M, Niizato K, Arai H. Relative paucity of tau accumulation in the small areas with abundant Abeta42-positive capillary amyloid angiopathy within a given cortical region in the brain of patients with Alzheimer pathology. *Acta Neuropathol*. 2006;111(6):510-518. doi:10.1007/s00401-006-0070-z
75. Weller RO, Boche D, Nicoll JA. Microvasculature changes and cerebral amyloid angiopathy in Alzheimer's disease and their potential impact on therapy. *Acta Neuropathol*. 2009;118(1):87-102. doi:10.1007/s00401-009-0498-z
76. Attems J, Jellinger KA. Only cerebral capillary amyloid angiopathy correlates with Alzheimer pathology--a pilot study. *Acta Neuropathol*. 2004;107(2):83-90. doi:10.1007/s00401-003-0796-9

77. Hecht M, Krämer LM, von Arnim CAF, Otto M, Thal DR. Capillary cerebral amyloid angiopathy in Alzheimer's disease: association with allocortical/hippocampal microinfarcts and cognitive decline. *Acta Neuropathol.* 2018;135(5):681-694. doi:10.1007/s00401-018-1834-y
78. Preston SD, Steart PV, Wilkinson A, Nicoll JA, Weller RO. Capillary and arterial cerebral amyloid angiopathy in Alzheimer's disease: defining the perivascular route for the elimination of amyloid beta from the human brain. *Neuropathol Appl Neurobiol.* 2003;29(2):106-117. doi:10.1046/j.1365-2990.2003.00424.x
79. Cipolla MJ. *The Cerebral Circulation.* San Rafael (CA): Morgan & Claypool Life Sciences; 2009.
80. Kalaria RN. Cerebral vessels in ageing and Alzheimer's disease. *Pharmacol Ther.* 1996;72(3):193-214. doi:10.1016/s0163-7258(96)00116-7
81. Chandra A, Li WA, Stone CR, Geng X, Ding Y. The cerebral circulation and cerebrovascular disease I: Anatomy. *Brain Circ.* 2017;3(2):45-56. doi:10.4103/bc.bc\_10\_17
82. Nishimura N, Schaffer CB, Friedman B, Lyden PD, Kleinfeld D. Penetrating arterioles are a bottleneck in the perfusion of neocortex. *Proc Natl Acad Sci U S A.* 2007;104(1):365-370. doi:10.1073/pnas.0609551104
83. Zlokovic BV. Neurovascular mechanisms of Alzheimer's neurodegeneration. *Trends Neurosci.* 2005;28(4):202-208. doi:10.1016/j.tins.2005.02.001
84. Zlokovic BV. The blood-brain barrier in health and chronic neurodegenerative disorders. *Neuron.* 2008;57(2):178-201. doi:10.1016/j.neuron.2008.01.003
85. Attwell D, Mishra A, Hall CN, O'Farrell FM, Dalkara T. What is a pericyte?. *J Cereb Blood Flow Metab.* 2016;36(2):451-455. doi:10.1177/0271678X15610340
86. Faraci FM, Heistad DD. Regulation of large cerebral arteries and cerebral microvascular pressure. *Circ Res.* 1990;66(1):8-17. doi:10.1161/01.res.66.1.8
87. Johnson, PC. The myogenic response. In: Handbook of Physiology. The Cardiovascular System. Vascular Smooth Muscle, Section 2, Vol. II. Bethesda, MD: American Physiological Society, 1981: pp. 409–442.
88. Van Nostrand WE, Melchor JP, Cho HS, Greenberg SM, Rebeck GW. Pathogenic effects of D23N Iowa mutant amyloid beta -protein. *J Biol Chem.* 2001;276(35):32860-32866. doi:10.1074/jbc.M104135200
89. Kisler K, Nelson AR, Montagne A, Zlokovic BV. Cerebral blood flow regulation and neurovascular dysfunction in Alzheimer disease. *Nat Rev Neurosci.* 2017;18(7):419-434. doi:10.1038/nrn.2017.48
90. LaFerla FM, Green KN. Animal models of Alzheimer disease. *Cold Spring Harb Perspect Med.* 2012;2(11):a006320. Published 2012 Nov 1. doi:10.1101/cshperspect.a006320
91. Sasaguri H, Nilsson P, Hashimoto S, Nagata K, Saito T, De Strooper B, Hardy J, Vassar R, Winblad B, Saido TC. APP mouse models for Alzheimer's disease preclinical studies. *EMBO J.* 2017;36(17):2473-2487. doi:10.15252/embj.201797397
92. Götz J, Bodea LG, Goedert M. Rodent models for Alzheimer disease. *Nat Rev Neurosci.* 2018 Oct;19(10):583-598. doi: 10.1038/s41583-018-0054-8. PMID: 30194347.

93. Hall AM, Roberson ED. Mouse models of Alzheimer's disease. *Brain Res Bull.* 2012;88(1):3-12. doi:10.1016/j.brainresbull.2011.11.017
94. Zhu XC, Tan L, Wang HF, Jiang T, Cao L, Wang C, Wang J, Tan CC, Meng XF, Yu JT. Rate of early onset Alzheimer's disease: a systematic review and meta-analysis [published correction appears in *Ann Transl Med.* 2016 May;4(9):E4]. *Ann Transl Med.* 2015;3(3):38. doi:10.3978/j.issn.2305-5839.2015.01.19
95. Jankowsky JL, Zheng H. Practical considerations for choosing a mouse model of Alzheimer's disease. *Mol Neurodegener.* 2017;12(1):89. Published 2017 Dec 22. doi:10.1186/s13024-017-0231-7
96. Dubal DB, Broestl L, Worden K. Sex and gonadal hormones in mouse models of Alzheimer's disease: what is relevant to the human condition?. *Biol Sex Differ.* 2012;3(1):24. Published 2012 Nov 5. doi:10.1186/2042-6410-3-24
97. Oakley H, Cole SL, Logan S, Maus E, Shao P, Craft J, Guillozet-Bongaarts A, Ohno M, Disterhoft J, Van Eldik L, Berry R, Vassar R. Intraneuronal beta-amyloid aggregates, neurodegeneration, and neuron loss in transgenic mice with five familial Alzheimer's disease mutations: potential factors in amyloid plaque formation. *J Neurosci.* 2006;26(40):10129-10140. doi:10.1523/JNEUROSCI.1202-06.2006
98. Gade Malmos K, Blancas-Mejia LM, Weber B, Buchner J, Ramirez-Alvarado M, Naiki H, Otzen D. ThT 101: a primer on the use of thioflavin T to investigate amyloid formation. *Amyloid.* 2017;24(1):1-16. doi:10.1080/13506129.2017.1304905
99. Cummings BJ, Mason AJ, Kim RC, Sheu PC, Anderson AJ. Optimization of techniques for the maximal detection and quantification of Alzheimer's-related neuropathology with digital imaging. *Neurobiol Aging.* 2002;23(2):161-170. doi:10.1016/s0197-4580(01)00316-5
100. Tsai W. H., "Moment-preserving thresholding: A new approach," *Comput. Vis. Graph. Image Process.* 1985;29:377-393. doi:10.1016/0734-189X(85)90133-1
101. Zack GW, Rogers WE, Latt SA. Automatic measurement of sister chromatid exchange frequency. *J Histochem Cytochem.* 1977;25(7):741-753. doi:10.1177/25.7.70454
102. Prewitt JM, Mendelsohn ML. The analysis of cell images. *Ann N Y Acad Sci.* 1966;128(3):1035-1053. doi:10.1111/j.1749-6632.1965.tb11715.x
103. Bhattacharya S, Haertel C, Maelicke A, Montag D. Galantamine slows down plaque formation and behavioral decline in the 5XFAD mouse model of Alzheimer's disease. *PLoS One.* 2014;9(2):e89454.
104. Reid GA, Darvesh S. Butyrylcholinesterase-knockout reduces brain deposition of fibrillar  $\beta$ -amyloid in an Alzheimer mouse model. *Neuroscience.* 2015;298:424-435.
105. Sadleir KR, Eimer WA, Cole SL, Vassar R. A $\beta$  reduction in BACE1 heterozygous null 5XFAD mice is associated with transgenic APP level. *Mol Neurodegener.* 2015;10:1.
106. Wittnam JL, Portelius E, Zetterberg H, Gustavsson MK, Schilling S, Koch B, Demuth HU, Blennow K, Wirths O, Bayer TA. Pyroglutamate amyloid  $\beta$  (A $\beta$ ) aggravates behavioral deficits in transgenic amyloid mouse model for Alzheimer disease. *J Biol Chem.* 2012;287(11):8154-8162. doi:10.1074/jbc.M111.308601
107. Frost JL, Le KX, Cynis H, Ekpo E, Kleinschmidt M, Palmour RM, Ervin FR, Snigdha S, Cotman CW, Saido TC, Vassar RJ, St George-Hyslop P, Ikezu T, Schilling S, Demuth HU, Lemere CA. Pyroglutamate-

- 3 amyloid- $\beta$  deposition in the brains of humans, non-human primates, canines, and Alzheimer disease-like transgenic mouse models. *Am J Pathol.* 2013;183(2):369-381. doi:10.1016/j.ajpath.2013.05.005
108. Jawhar S, Wirths O, Schilling S, Graubner S, Demuth HU, Bayer TA. Overexpression of glutaminyl cyclase, the enzyme responsible for pyroglutamate A $\beta$  formation, induces behavioral deficits, and glutaminyl cyclase knock-out rescues the behavioral phenotype in 5XFAD mice. *J Biol Chem.* 2011;286(6):4454-4460. doi:10.1074/jbc.M110.185819
109. Dassen H, Punyadeera C, Kamps R, Klomp J, Dunselman G, Dijcks F, de Goeij A, Ederveen A, Groothuis P. Progesterone regulation of implantation-related genes: new insights into the role of oestrogen. *Cell Mol Life Sci.* 2007;64(7-8):1009-1032. doi:10.1007/s00018-007-6553-9
110. Smith LC, Moreno S, Robertson L, Robinson S, Gant K, Bryant AJ, Sabo-Attwood T. Transforming growth factor beta1 targets estrogen receptor signaling in bronchial epithelial cells. *Respir Res.* 2018;19(1):160. Published 2018 Aug 30. doi:10.1186/s12931-018-0861-5
111. Tang MX, Jacobs D, Stern Y, Marder K, Schofield P, Gurland B, Andrews H, Mayeux R. Effect of oestrogen during menopause on risk and age at onset of Alzheimer's disease. *Lancet.* 1996;348(9025):429-432. doi:10.1016/S0140-6736(96)03356-9
112. Paganini-Hill A, Henderson VW. Estrogen deficiency and risk of Alzheimer's disease in women. *Am J Epidemiol.* 1994;140(3):256-261. doi:10.1093/oxfordjournals.aje.a117244
113. Ziegler-Waldkirch S, Marksteiner K, Stoll J, et al. Environmental enrichment reverses A $\beta$  pathology during pregnancy in a mouse model of Alzheimer's disease. *Acta Neuropathol Commun.* 2018;6(1):44. Published 2018 May 31.
114. Prange-Kiel J, Dudzinski DA, Pröls F, Glatzel M, Matschke J, Rune GM. Aromatase Expression in the Hippocampus of AD Patients and 5xFAD Mice. *Neural Plast.* 2016;2016:9802086.
115. Hirata-Fukae C, Li HF, Hoe HS, Gray AJ, Minami SS, Hamada K, Niikura T, Hua F, Tsukagoshi-Nagai H, Horikoshi-Sakuraba Y, Mughal M, Rebeck GW, LaFerla FM, Mattson MP, Iwata N, Saido TC, Klein WL, Duff KE, Aisen PS, Matsuoka Y. Females exhibit more extensive amyloid, but not tau, pathology in an Alzheimer transgenic model. *Brain Res.* 2008;1216:92-103. doi:10.1016/j.brainres.2008.03.079
116. Oddo S, Caccamo A, Shepherd JD, Murphy MP, Golde TE, Kaye R, Metherate R, Mattson MP, Akbari Y, LaFerla FM. Triple-transgenic model of Alzheimer's disease with plaques and tangles: intracellular Abeta and synaptic dysfunction. *Neuron.* 2003;39(3):409-421. doi:10.1016/s0896-6273(03)00434-3
117. Jiao SS, Bu XL, Liu YH, Zhu C, Wang QH, Shen LL, Liu CH, Wang YR, Yao XQ, Wang YJ.. Sex Dimorphism Profile of Alzheimer's Disease-Type Pathologies in an APP/PS1 Mouse Model. *Neurotox Res.* 2016;29(2):256-266. doi:10.1007/s12640-015-9589-x
118. Radde R, Bolmont T, Kaeser SA, Coomaraswamy J, Lindau D, Stoltze L, Calhoun ME, Jäggi F, Wolburg H, Gengler S, Haass C, Ghetti B, Czech C, Hölscher C, Mathews PM, Jucker M. Abeta42-driven cerebral amyloidosis in transgenic mice reveals early and robust pathology. *EMBO Rep.* 2006;7(9):940-946. doi:10.1038/sj.embor.7400784

119. Overk CR, Lu PY, Wang YT, Choi J, Shaw JW, Thatcher GR, Mufson EJ. Effects of aromatase inhibition versus gonadectomy on hippocampal complex amyloid pathology in triple transgenic mice. *Neurobiol Dis.* 2012;45(1):479-487. doi:10.1016/j.nbd.2011.08.035
120. Carroll JC, Rosario ER, Chang L, Stanczyk FZ, Oddo S, LaFerla FM, Pike CJ. Progesterone and estrogen regulate Alzheimer-like neuropathology in female 3xTg-AD mice. *J Neurosci.* 2007;27(48):13357-13365. doi:10.1523/JNEUROSCI.2718-07.2007
121. Devi L, Alldred MJ, Ginsberg SD, Ohno M. Sex- and brain region-specific acceleration of  $\beta$ -amyloidogenesis following behavioral stress in a mouse model of Alzheimer's disease. *Mol Brain.* 2010;3:34. Published 2010 Nov 8. doi:10.1186/1756-6606-3-34
122. Caroni P. Overexpression of growth-associated proteins in the neurons of adult transgenic mice. *J Neurosci Methods.* 1997;71(1):3-9. doi:10.1016/s0165-0270(96)00121-5
123. Porrero C, Rubio-Garrido P, Avendaño C, Clascá F. Mapping of fluorescent protein-expressing neurons and axon pathways in adult and developing Thy1-eYFP-H transgenic mice. *Brain Res.* 2010;1345:59-72. doi:10.1016/j.brainres.2010.05.061
124. Haeryfar SM, Hoskin DW. Thy-1: more than a mouse pan-T cell marker. *J Immunol.* 2004;173(6):3581-3588. doi:10.4049/jimmunol.173.6.3581
125. Yoon SS, Jo SA. Mechanisms of Amyloid- $\beta$  Peptide Clearance: Potential Therapeutic Targets for Alzheimer's Disease. *Biomol Ther (Seoul).* 2012;20(3):245-255. doi:10.4062/biomolther.2012.20.3.245
126. Bartolini M, Bertucci C, Bolognesi ML, Cavalli A, Melchiorre C, Andrisano V. Insight into the kinetic of amyloid beta (1-42) peptide self-aggregation: elucidation of inhibitors' mechanism of action. *Chembiochem.* 2007;8(17):2152-2161. doi:10.1002/cbic.200700427
127. Kawarabayashi T, Younkin LH, Saido TC, Shoji M, Ashe KH, Younkin SG. Age-dependent changes in brain, CSF, and plasma amyloid (beta) protein in the Tg2576 transgenic mouse model of Alzheimer's disease. *J Neurosci.* 2001;21(2):372-381. doi:10.1523/JNEUROSCI.21-02-00372.2001
128. Kim TK, Lee JE, Park SK, Lee KW, Seo JS, Im JY, Kim ST, Lee JY, Kim YH, Lee JK, Han PL. Analysis of differential plaque depositions in the brains of Tg2576 and Tg-APP<sup>swe</sup>/PS1<sup>dE9</sup> transgenic mouse models of Alzheimer disease. *Exp Mol Med.* 2012;44(8):492-502. doi:10.3858/em.2012.44.8.056
129. Rockenstein E, Mallory M, Mante M, Sisk A, Masliah E. Early formation of mature amyloid-beta protein deposits in a mutant APP transgenic model depends on levels of A $\beta$ (1-42). *J Neurosci Res.* 2001;66(4):573-582. doi:10.1002/jnr.1247
130. Naiki H, Higuchi K, Hosokawa M, Takeda T. Fluorometric determination of amyloid fibrils in vitro using the fluorescent dye, thioflavin T1. *Anal Biochem.* 1989;177(2):244-249. doi:10.1016/0003-2697(89)90046-8
131. Sen P, Fatima S, Ahmad B, Khan RH. Interactions of thioflavin T with serum albumins: spectroscopic analyses. *Spectrochim Acta A Mol Biomol Spectrosc.* 2009;74(1):94-99. doi:10.1016/j.saa.2009.05.010
132. Harel M, Sonoda LK, Silman I, Sussman JL, Rosenberry TL. Crystal structure of thioflavin T bound to the peripheral site of Torpedo californica acetylcholinesterase reveals how thioflavin T acts as a sensitive fluorescent reporter of ligand binding to the acylation site. *J Am Chem Soc.* 2008;130(25):7856-7861. doi:10.1021/ja7109822

133. Hatami A, Albay R 3rd, Monjazez S, Milton S, Glabe C. Monoclonal antibodies against A $\beta$ 42 fibrils distinguish multiple aggregation state polymorphisms in vitro and in Alzheimer disease brain. *J Biol Chem*. 2014;289(46):32131-32143. doi:10.1074/jbc.M114.594846
134. Wisniewski HM, Wen GY, Kim KS. Comparison of four staining methods on the detection of neuritic plaques. *Acta Neuropathol*. 1989;78(1):22-27. doi:10.1007/BF00687398
135. Xu F, Kotarba AE, Ou-Yang MH, Fu Z, Davis J, Smith SO, Van Nostrand WE. Early-onset formation of parenchymal plaque amyloid abrogates cerebral microvascular amyloid accumulation in transgenic mice. *J Biol Chem*. 2014;289(25):17895-17908. doi:10.1074/jbc.M113.536565
136. Giannoni P, Arango-Lievano M, Neves ID, Rousset MC, Baranger K, Rivera S, Jeanneteau F, Claeysen S, Marchi N. Cerebrovascular pathology during the progression of experimental Alzheimer's disease. *Neurobiol Dis*. 2016;88:107-117. doi:10.1016/j.nbd.2016.01.001
137. Spangenberg E, Severson PL, Hohsfield LA, Crapser J, Zhang J, Burton EA, Zhang Y, Spevak W, Lin J, Phan NY, Habets G, Rymar A, Tsang G, Walters J, Nespi M, Singh P, Broome S, Ibrahim P, Zhang C, Bollag G, West BL, Green KN. Sustained microglial depletion with CSF1R inhibitor impairs parenchymal plaque development in an Alzheimer's disease model. *Nat Commun*. 2019;10(1):3758. Published 2019 Aug 21. doi:10.1038/s41467-019-11674-z
138. Ahn KC, Learman CR, Dunbar GL, Maiti P, Jang WC, Cha HC, Song MS. Characterization of Impaired Cerebrovascular Structure in APP/PS1 Mouse Brains. *Neuroscience*. 2018;385:246-254. doi:10.1016/j.neuroscience.2018.05.002
139. Xu W, Xu F, Anderson ME, Kotarba AE, Davis J, Robinson JK, Van Nostrand WE. Cerebral microvascular rather than parenchymal amyloid- $\beta$  protein pathology promotes early cognitive impairment in transgenic mice. *J Alzheimers Dis*. 2014;38(3):621-632. doi:10.3233/JAD-130758
140. O'Leary TP, Mantolino HM, Stover KR, Brown RE. Age-related deterioration of motor function in male and female 5xFAD mice from 3 to 16 months of age. *Genes Brain Behav*. 2020;19(3):e12538.
141. Jawhar S, Trawicka A, Jenneckens C, Bayer TA, Wirths O. Motor deficits, neuron loss, and reduced anxiety coinciding with axonal degeneration and intraneuronal A $\beta$  aggregation in the 5XFAD mouse model of Alzheimer's disease. *Neurobiol Aging*. 2012;33(1):196.e29-196.e1.96E40. doi:10.1016/j.neurobiolaging.2010.05.027
142. Wu D, Tang X, Gu LH, Li XL, Qi XY, Bai F, Chen XC, Wang JZ, Ren QG, Zhang ZJ. LINGO-1 antibody ameliorates myelin impairment and spatial memory deficits in the early stage of 5XFAD mice. *CNS Neurosci Ther*. 2018;24(5):381-393. doi:10.1111/cns.12809
143. Gu L, Wu D, Tang X, Qi X, Li X, Bai F, Chen X, Ren Q, Zhang Z. Myelin changes at the early stage of 5XFAD mice. *Brain Res Bull*. 2018;137:285-293. doi:10.1016/j.brainresbull.2017.12.013
144. Richard BC, Kurdakova A, Baches S, Bayer TA, Weggen S, Wirths O. Gene Dosage Dependent Aggravation of the Neurological Phenotype in the 5XFAD Mouse Model of Alzheimer's Disease. *J Alzheimers Dis*. 2015;45(4):1223-1236. doi:10.3233/JAD-143120